Determining soil moisture and soil properties in vegetated areas by assimilating soil temperatures

Dong, Jianzhi; Steele-Dunne, Susan C.; Ochsner, Tyson E.; van de Giesen, Nick

DOI
10.1002/2015WR018425

Publication date
2016

Document Version
Final published version

Published in
Water Resources Research

Citation (APA)
Dong, J., Steele-Dunne, S. C., Ochsner, T. E., & van de Giesen, N. (2016). Determining soil moisture and soil properties in vegetated areas by assimilating soil temperatures. *Water Resources Research*, *52*(6), 4280-4300. https://doi.org/10.1002/2015WR018425

AGU PUBLICATIONS

Water Resources Research

RESEARCH ARTICLE
10.1002/2015WR018425

Determining soil moisture and soil properties in vegetated areas by assimilating soil temperatures

Jianzhi Dong[1], Susan C. Steele-Dunne[1], Tyson E. Ochsner[2], and Nick van de Giesen[1]

[1]Water Resources Section, Faculty of Civil Engineering and Geosciences, Delft University of Technology, Delft, Netherlands, [2]Department of Plant and Soil Sciences, Oklahoma State University, Stillwater, Oklahoma, USA

Key Points:
- We improved the state of art vadose zone model by coupling a surface energy scheme
- We highlighted soil temperature can be used to detect of soil moisture and property variability
- We demonstrated observation depth can be jointly estimated with model states and parameters

Supporting Information:
- Supporting Information S1

Correspondence to:
J. Dong,
jianzhi.dong@tudelft.nl

Citation:
Dong, J., S. C. Steele-Dunne, T. E. Ochsner, and N. van de Giesen (2016), Determining soil moisture and soil properties in vegetated areas by assimilating soil temperatures, *Water Resour. Res.*, *52*, 4280–4300, doi:10.1002/2015WR018425.

Received 25 NOV 2015
Accepted 11 MAY 2016
Accepted article online 17 MAY 2016
Published online 3 JUN 2016

Abstract This study addresses two critical barriers to the use of Passive Distributed Temperature Sensing (DTS) for large-scale, high-resolution monitoring of soil moisture. In recent research, a particle batch smoother (PBS) was developed to assimilate sequences of temperature data at two depths into Hydrus-1D to estimate soil moisture as well as soil thermal and hydraulic properties. However, this approach was limited to bare soil and assumed that the cable depths were perfectly known. In order for Passive DTS to be more broadly applicable as a soil hydrology research and remote sensing soil moisture product validation tool, it must be applicable in vegetated areas. To address this first limitation, the forward model (Hydrus-1D) was improved through the inclusion of a canopy energy balance scheme. Synthetic tests were used to demonstrate that without the canopy energy balance scheme, the PBS estimated soil moisture could be even worse than the open loop case (no assimilation). When the improved Hydrus-1D model was used as the forward model in the PBS, vegetation impacts on the soil heat and water transfer were well accounted for. This led to accurate and robust estimates of soil moisture and soil properties. The second limitation is that, cable depths can be highly uncertain in DTS installations. As Passive DTS uses the downward propagation of heat to extract moisture-related variations in thermal properties, accurate estimates of cable depths are essential. Here synthetic tests were used to demonstrate that observation depths can be jointly estimated with other model states and parameters. The state and parameter results were only slightly poorer than those obtained when the cable depths were perfectly known. Finally, in situ temperature data from four soil profiles with different, but known, soil textures were used to test the proposed approach. Results show good agreement between the observed and estimated soil moisture, hydraulic properties, thermal properties, and observation depths at all locations. The proposed method resulted in soil moisture estimates in the top 10 cm with RMSE values typically $<0.04\ m^3/m^3$. This demonstrates the potential of detecting the spatial variability of soil moisture and properties in vegetated areas from Passive DTS data.

1. Introduction

Interactions between the land surface and the atmosphere are strongly influenced by soil moisture [*Entekhabi et al.*, 1996]. Thus, development of global, remotely sensed soil moisture products has been a major research focus in recent years [e.g., *Wagner et al.*, 1999; *Entekhabi et al.*, 2010; *Kerr et al.*, 2001; *Owe et al.*, 2008]. In order to calibrate and validate these remote sensing products, large-scale in situ soil moisture measurements are needed [*Crow et al.*, 2012; *Ochsner et al.*, 2013]. In situ soil moisture measurement at the scale of a satellite footprint is challenging using traditional point-scale measurement methods, and several novel methods have been proposed to circumvent the need for intensive point-scale measurements [*Ochsner et al.*, 2013]. Examples include cosmic ray probes [*Zreda et al.*, 2008], GPS reflectometry [*Larson et al.*, 2008], and Distributed Temperature Sensing (DTS) [*Steele-Dunne et al.*, 2010; *Sayde et al.*, 2010]. DTS is an advanced environmental temperature measurement technique using fiber-optic cables. It can provide continuous temperature measurements at high resolutions (temporal resolution <1 min and spatial resolution <1 m), and cables can easily extend to kilometers in length [*Selker et al.*, 2006]. DTS may have the potential to provide submeter resolution soil moisture measurements up to kilometers. Hence, it may provide insights about soil moisture variability across different scales [*Ochsner et al.*, 2013].

The key to DTS methods is to link the measured soil temperature or thermal responses to soil moisture. One category of DTS techniques is Active DTS, in which electrically generated heat pulses are applied to the

fiber-optic cables. The temperature change during and after the heat pulse can be related to soil moisture using either empirically calibrated or physically based equations [*Sayde et al*., 2010; *Striegl et al*., 2012; *Ciocca et al*., 2012]. The Active DTS method has been shown to be accurate, particularly when soil moisture is low. However, the large energy requirement for heat pulses is a logistical obstacle for some field experiments. To circumvent this problem, *Steele-Dunne et al*. [2010] investigated the feasibility of using DTS measured soil thermal responses to the net radiation (Passive DTS). In their study, soil heat transfer between two measurement depths was assumed to be due to heat diffusion. An "inversion method" was used to determine the value of soil thermal diffusivity that provides the best fit to the observed soil temperatures. Provided the thermal diffusivity-soil moisture relationship is known, soil moisture can be estimated every meter along the fiber-optic cables. Their study also highlighted several key challenges in applying an inversion method to DTS. First, the uncertainties in the thermal diffusivity-soil moisture relationship may significantly affect the accuracy of the estimated soil moisture. Second, thermal diffusivity is relatively insensitive to soil moisture for wet soils, which means the estimates are not reliable when soil moisture is high. Third, the inversion method may fail to converge to a reasonable value when solar radiation is low. Finally, the approach is very sensitive to the uncertainties of the cable depths.

Recently, *Dong et al*. [2015a] demonstrated that data assimilation could be used to address several challenges in estimating soil moisture using passively measured soil temperatures. Data assimilation can optimally combine model estimates and observations [*Reichle*, 2008], in which different source of uncertainties can be considered [*Liu and Gupta*, 2007]. The Ensemble Kalman Filter (EnKF) is one of the most popular data assimilation techniques, it assumes the prior distribution and the observation error are normally distributed [*Evensen*, 1994]. The posterior distribution is then solved analytically. The EnKF is shown to be a robust data assimilation technique, which can be easily implemented in complex systems [*Evensen*, 2009]. The EnKF is capable of constraining hydrologic estimates when remote sensing observations are assimilated, e.g., in improving footprint scale soil moisture estimates [e.g., *Margulis et al*., 2002; *Reichle et al*., 2004; *Reichle and Koster*, 2005; *Crow et al*., 2008; *Draper et al*., 2012; *Qin et al*., 2009; *Yu et al*., 2012], terrestrial water storage [e.g., *Zaitchik et al*., 2008; *Forman et al*., 2012; *Forman and Reichle*, 2013], and stream flow estimates [e.g., *Clark et al*., 2008; *Crow and Ryu*, 2009; *Rafieeinasab et al*., 2014; *Rakovec et al*., 2012].

Dong et al. [2015a] used a fully coupled soil water, heat and vapor transfer model as the forward model (Hydrus-1D) [*Simunek et al*., 2009] and then applied the EnKF was to update the prior estimated soil moisture sequentially using soil temperatures. A series of synthetic experiments were used to demonstrate that the data assimilation method could handle uncertainties in soil texture (soil thermal diffusivity-moisture curve). Furthermore, even if net radiation was low and the soil temperature contains little information on soil moisture, the EnKF produced a reasonable soil moisture value from the forward model.

Series of soil temperature measurements contain more information about the soil heating and cooling rate, and therefore may contain more information about soil moisture [*Boni et al*., 2001; *Bateni and Entekhabi*, 2012; *Caparrini et al*., 2003]. This implies that batch smoothing, rather than sequential filtering is more suitable for soil moisture estimation using soil temperatures. The Ensemble Smoother (ES) is similar to the EnKF, except that observations are assimilated in a batch to update all states within some window in time. This allows the ES to consider observations beyond the estimation time. The ES has been shown to be suitable for estimating land surface soil moisture states by assimilating microwave remote sensing observations [*Dunne and Entekhabi*, 2005]. However, the ES may be inaccurate when the system is highly nonlinear or the prior distribution is not normally distributed [*Van Leeuwen and Evensen*, 1996]. *Dong et al*. [2015b] presented a so-called Particle Batch Smoother (PBS) to overcome this problem. The PBS is an extension of the well-established particle filter (PF) [*Moradkhani et al*., 2005a, 2012; *Montzka et al*., 2011, 2013a, 2013b; *Dumedah and Coulibaly*, 2013; *Noh et al*., 2014]. Similar to the PF algorithm, the PBS maps the prior distribution using randomly sampled points, rather than only preserve the mean and the standard deviation of the prior in the EnKF [*Moradkhani et al*., 2005a; *Dong et al*., 2015b; *Margulis et al*., 2015]. Similar to the ES, the PBS state and observations are distributed in time so that observations within some window are used to update states in that window.

Dong et al. [2015b] used the PBS to update the soil moisture using the soil temperature evolution within a window of a fixed length. They showed that the PBS outperforms sequential filtering methods. Previous studies [*Yan et al*., 2015; *Montzka et al*., 2011] have demonstrated that updating soil moisture and properties jointly using the PF leads to significantly improved estimates compared to the case that updates the model states alone. Instead of using microwave remote sensing observations [*Yan et al*., 2015; *Montzka et al*., 2011],

Dong et al. [2016] demonstrated that soil hydraulic properties could be accurately estimated by assimilating soil temperature observations with the PBS. This results in an improved water retention curve compared to the open loop, which benefits the performance of the forward model and in turn improves the soil moisture estimates. Soil temperature estimates were also discussed in detail by *Dong et al*. [2016]. It was shown that the soil temperature profile can already be well estimated when only model states are updated, since soil temperature at two shallow depths are directly observed, and highly correlated at different depths. When the model parameters and states are jointly updated, the improved model parameters can significantly benefit the performance of the forward model, which yields further improvements in soil temperature estimates at depth.

Though significant progress has been made in the Passive DTS method through the application of data assimilation, two key challenges remain. First, the forward model (Hydrus-1D) cannot simulate energy balance processes in vegetated areas. Hence, previous studies were limited to bare soils. This severely limits the usefulness of the approach in hydrological sciences and as a validation tool for remote sensing. Further, the observation depths were assumed to be perfectly known. This assumption is rarely valid in DTS applications [*Steele-Dunne et al*., 2010]. To tackle these challenges, this study will first improve the existing forward model (Hydrus-1D) by including a canopy energy balance scheme. Then, we will propose a method that can estimate the observation depths as part of the data assimilation scheme. In the following sections, we will demonstrate the importance of including the canopy energy balance scheme in the forward model using synthetic experiments. The performance of the algorithm that jointly estimates the observation depth, model parameters and states will also be evaluated using synthetic experiments. Finally, the new approach will be tested using real-world observations.

2. Method and Materials

2.1. Modified Hydrus-1D Model

2.1.1. Soil Water, Heat, and Vapor Transfer

In this study, the vertical soil water, heat and vapor transport processes in the unsaturated zone are simulated using Hydrus-1D [*Saito et al*., 2006]. The governing equation for one-dimensional liquid and vapor flow is expressed as

$$\frac{\partial\theta}{\partial t}=\frac{\partial}{\partial z}\left[K_{Th}\frac{\partial h}{\partial z}+K_{Lh}+K_{TT}\frac{\partial T}{\partial z}\right]-S \tag{1}$$

where θ is soil water content ($m^3\ m^{-3}$) at time t (s), and z is the vertical coordinate (positive upward) (m). K_{Th} and K_{TT} are the isothermal and thermal total hydraulic conductivities, respectively, and K_{Lh} is the isothermal unsaturated hydraulic conductivity. S is a sink term ($m^3\ m^{-3}\ s^{-1}$), which in this case is the water taken up by the roots. The integral of S is then the transpiration rate, which will be estimated in the next section. K_{Lh} and the soil retention curve are determined using van Genuchten's model [*Van Genuchten*, 1980]:

$$K_{Lh}=K_sS_e^l\left[1-\left(1-S_e^{\frac{1}{m}}\right)^m\right]^2 \tag{2}$$

$$\theta(h)=\begin{cases}\theta_r+\dfrac{\theta_s-\theta_r}{\left[1+|\alpha h|^n\right]^m} & h<0\\ \theta_s & h\geq 0\end{cases} \tag{3}$$

where K_s is the saturated hydraulic conductivity ($m\ s^{-1}$), S_e is the effective saturation, l, m, n, and α are empirical shape parameters and θ_r and θ_s are the residual and saturated soil water contents ($m^3\ m^{-3}$). The governing equation for soil heat transport is

$$\begin{aligned}&\frac{\partial C_pT}{\partial t}+L_0\frac{\partial\theta_v}{\partial t}=\\&\frac{\partial}{\partial z}\left[\lambda(\theta)\frac{\partial T}{\partial z}\right]-C_w\frac{\partial q_LT}{\partial z}\\&-L_0\frac{\partial q_v}{\partial z}-C_v\frac{\partial q_vT}{\partial z}-C_wST\end{aligned} \tag{4}$$

where T is soil temperature (K), C_w, C_v, and C_p are the volumetric heat capacities of water, vapor, and moist soil ($J\ m^{-3}\ K^{-1}$), L_0 is the volumetric latent heat of vaporization of liquid water ($J\ m^{-3}$), q_L and q_v are the

flux densities of liquid water and vapor (m s^{-1}), and $\lambda(\theta)$ is apparent soil thermal conductivity (W m^{-1} K^{-1}). $\lambda(\theta)$ is estimated from

$$\lambda(\theta)=\lambda_0(\theta)+\beta C_w|q_L| \tag{5}$$

where β is the thermal dispersivity (m). In this modified Hydrus-1D model, thermal conductivity λ_0 is estimated using the model proposed by *Lu et al*. [2007]. The Lu model is expressed as

$$\lambda_0(\theta)=(\lambda_{sat}-\lambda_{dry})K_e+\lambda_{dry} \tag{6}$$

where K_e is the Kersten number, and λ_{dry} and λ_{sat} are soil thermal conductivities for dry and saturate soil, respectively. The λ_{dry} is approximated as

$$\lambda_{dry}=-0.56\theta_s+0.51 \tag{7}$$

Note that the soil porosity is assumed to be equal to the saturated water content in this study. The parameter K_e is estimated as

$$K_e=\exp\left[\alpha_T-\alpha_T\left(\frac{\theta}{\theta_s}\right)^{\alpha_T-1.33}\right] \tag{8}$$

where α_T is a soil texture dependent parameter ranging from 0.27 to 0.96.

2.1.2. Canopy Energy Balance

The soil surface energy balance scheme used in the modified Hydrus-1D is based on that presented by *Oleson et al*. [2010]. The surface energy balance equations for the vegetation and ground are as follows:

$$\vec{S}_v-\vec{L}_v=H_v+\lambda E_v \tag{9}$$

$$\vec{S}_g-\vec{L}_g=H_g+\lambda E_g+G \tag{10}$$

where $\vec{S}_v$ is the solar radiation absorbed by the vegetation canopy, $\vec{L}_v$ is the net longwave radiation for the vegetation canopy (positive upward from the canopy), and $\vec{S}_g$ and $\vec{L}_g$ are defined similarly such that $\vec{S}_g-\vec{L}_g$ is the net radiation at the ground surface. The radiation terms were estimated using the radiative transfer model proposed by *Sellers* [1985]. H_v and λE_v are the sensible and latent heat fluxes from the canopy, H_g and λE_g are the sensible and latent heat fluxes from the ground, $\lambda \approx 2.501 \times 10^6$ J kg^{-1}, and G is the ground heat flux [*Oleson et al*., 2010]. All the energy fluxes have a unit of W m^{-2}. The water vapor flux from canopy (i.e., E_v, in kg s^{-1} m^{-2}) includes evaporation of intercepted water and transpiration.

The sensible heat fluxes are calculated as follows:

$$H_v=-\rho_{atm}C_p\frac{(T_s-T_v)}{r_b}(L_{leaf}+L_{stem}) \tag{11}$$

$$H_g=-\rho_{atm}C_p\frac{(T_s-T_g)}{r'_{ah}} \tag{12}$$

where ρ_{atm} is the density of air (kg m^{-3}), C_p is the specific heat capacity of air at constant pressure (J kg^{-1} K^{-1}), T_s, T_v, and T_g are the temperatures of canopy air (K), vegetation, and ground surface respectively, L_{leaf} and L_{stem} are the exposed leaf and stem area indices, r_b is the leaf boundary layer resistance (m s^{-1}), and r'_{ah} is the aerodynamic resistance to the sensible heat transfer between the ground surface and canopy air. Assuming the air within the vegetation canopy does not store heat, it gives

$$H=H_v+H_g \tag{13}$$

$$H=-\rho_{atm}C_p\frac{(\theta_{atm}-T_s)}{r_{ah}} \tag{14}$$

where θ_{atm} is the potential air temperature (K), and r_{ah} is the aerodynamic resistance to the sensible heat transfer from the atmosphere to the vegetated land surface. Combining equation (11) to equation (14), the temperature of the canopy air (T_s) can be estimated as

$$T_s = \frac{c_a^h \theta_{atm} + c_v^h T_v + c_g^h T_g}{c_v^h + c_a^h + c_g^h} \tag{15}$$

where $c_a^h = 1/r_{ah}$, $c_v^h = (L_{leaf} + L_{stem})/r_b$ and $c_g^h = 1/r'_{ah}$. Water vapor fluxes from the vegetation and soil surface are calculated using:

$$E_v = -\rho_{atm} \frac{(q_s - q_{sat}^{T_v})}{r_{total}} \tag{16}$$

$$E_g = -\rho_{atm} \frac{(q_s - q_g)}{r_{gw}} \tag{17}$$

where q_s is the specific humidity of the canopy air, q_g is the specific humidity at the ground surface, $q_{sat}^{T_v}$ is the saturation water vapor specific humidity at the vegetation temperature (kg kg^{-1}), r_{total} and r_{gw} are the resistances of the vapor transfer from the canopy and the ground surface to the canopy air, in m s^{-1}. Similar to the sensible heat flux, the water vapor flux is given by

$$E = -\rho_{atm} \frac{(q_{atm} - q_s)}{r_{aw}} \tag{18}$$

$$E = E_g + E_v \tag{19}$$

where q_{atm} is the specific humidity of the atmosphere, and r_{aw} is the aerodynamic resistance to vapor transfer in m s^{-1}. Combining equation (16) to equation (19), the specific humidity of the canopy air q_s is solved as

$$q_s = \frac{c_a^w q_{atm} + c_v^w q_{sat}^{T_v} + c_g^w q_g}{c_a^w + c_v^w + c_g^w} \tag{20}$$

where $c_a^w = 1/r_{aw}$, $c_g^w = 1/r_{gw}$, and $c_v^w = 1/r_{total}$. All the resistance and conductance terms were estimated using measured wind speed, relative humidity, air temperatures, and vegetation properties as outlined by *Bonan* [1996]. The initial vegetation parameters (e.g., vegetation optical and structural properties) were guessed to be the default values of "C3 grass" as prescribed in *Bonan* [1996].

To solve the energy fluxes (i.e., H_v, H_g, λE_v, λE_g, and G), iterations between the surface energy balance and the soil water, heat and vapor transport equation was required. The iteration procedure will provide the estimated T_v, resistances and the energy fluxes that satisfy the energy balance and the water balance at each time step. The details of the numerical implementation of the algorithm are provided by *Oleson et al.* [2010].

2.1.3. Boundary Condition and Model Settings

The upper boundary for the soil heat transfer is calculated using the energy balance equations as described in the previous section, and "zero gradient" is used as the lower boundary. The upper boundary of soil water movement is characterized by the liquid (precipitation) and vapor (evapotranspiration) water fluxes. During precipitation events, interception was estimated using the procedure provided by *Oleson et al.* [2010]. The lower boundary condition of the soil water movement model is set to "Free drainage" [*Simunek et al.*, 2009]. The model step in Hydrus-1D was automatically adjusted by the numerical convergence, which is approximately 1 min in this study. The soil column to 1 m depth is simulated with a vertical resolution of 1 cm.

2.2. The Particle Batch Smoother (PBS)

The model states of interest are soil moisture and temperature from the surface (0 m) to 1 m. An ensemble of model states is evolved in parallel using the forward model:

$$\mathbf{x}_t^i = f\left(\mathbf{x}_{t-1}^i, \mathbf{u}_t^i, \mathbf{b}_t^i\right) + \mathbf{w}_t^i \tag{21}$$

where $\mathbf{x}_t^i$ is a vector of the model states (θ and T in this study) of the ith particle at time t, $\mathbf{u}_t^i$ is the perturbed forcing data, $\mathbf{b}_t^i$ is a vector of model parameters, $\mathbf{w}_t^i$ is the model error, and f is the forward model (Hydrus-1D) [*Moradkhani et al.*, 2012; *DeChant and Moradkhani*, 2012].

The model estimates are related to the observations by

$$\widehat{\mathbf{y}}_t^i = h(\mathbf{x}_t^i) + \mathbf{v}_t^i \tag{22}$$

where $\widehat{\mathbf{y}}_t^i$ is the simulated observation vector, h is an operator relating the prior estimated states ($\mathbf{x}_t^i$) to the measured variable and $\mathbf{v}_t^i$ is the observation error [*Moradkhani et al*., 2012]. The vector $\widehat{\mathbf{y}}_t^i$ only contains soil temperatures, while the state vector $\widehat{\mathbf{x}}_t^i$ contains both soil simulated temperatures and moisture. The observation error is set to be 0.5°C. In this study, the observations are the temperatures at 5 and 10 cm.

The posterior distribution of interest is the joint distribution of the model states (i.e., soil temperature and moisture) and model parameters (i.e., soil thermal, hydraulic properties, and LAI) over a certain time interval (window length). The posterior distribution is mapped using particles with associated weights:

$$p(\mathbf{x}_{t-L+1:t}, \mathbf{b}_{t-L+1:t} | \mathbf{y}_{1:t}) = \sum_{i=1}^{N} w_t^i \delta\left(\mathbf{x}_{t-L+1:t} - \mathbf{x}_{t-L+1:t}^i, \mathbf{b}_t - \mathbf{b}_t^i\right) \tag{23}$$

where $\{x_{t-L+1:t}^i, \mathbf{b}_t^i\}$ denotes the ith particle, w_t^i is its weight, and δ is Dirac delta function [*Moradkhani et al*., 2005b], and L is the window length. The impact of window length and observation interval has already been discussed in a previous study [*Dong et al*., 2015b]. Because only hourly data are available, L is set to be 12 h in this study to ensure that there are sufficient observations for each batch window to estimate both the states and parameters. The parameters were assumed to be constant within each batch window, i.e., $\mathbf{b}_{t-L+1:t}^i = \mathbf{b}_t^i$. Similar to the particle filter algorithm, the PBS estimates the particle weights using importance sampling:

$$w_t^{i,*} \propto w_{t-L}^{i,*} \frac{p(\mathbf{x}_{t-L+1:t}^i | \mathbf{x}_{1:t-L}^i) p(\mathbf{y}_{t-L+1:t} | \mathbf{x}_{t-L+1:t}^i)}{q(\mathbf{x}_{t-L+1:t}^i | \mathbf{x}_{1:t-L}^i, \mathbf{y}_{1:t-L})} \tag{24}$$

where $w_t^{i,*}$ is the unnormalized particle weight, $q(\mathbf{x}_{t-L+1:t}^i | \mathbf{x}_{1:t-L}^i, \mathbf{y}_{1:t-L})$ is the proposal distribution for importance sampling, $p(\mathbf{x}_{t-L+1:t}^i | \mathbf{x}_{1:t-L}^i)$ is the transition prior, and $p(\mathbf{y}_{t-L+1:t} | \mathbf{x}_{t-L+1:t}^i)$ is the likelihood function, which is calculated as

$$p(\mathbf{y}_{t-L+1:t} | \mathbf{x}_{t-L+1:t}^i) = \prod_{j=t-L+1}^{t} \frac{1}{(2\pi)^{n_o/2} det(\mathbf{R})^{1/2}} e^{\left[-0.5\beta^2 (\mathbf{y}_j - \widehat{\mathbf{y}}_j^i)^T \mathbf{R}^{-1} (\mathbf{y}_j - \widehat{\mathbf{y}}_j^i)\right]} \tag{25}$$

where $\mathbf{R}$ is the error covariance of the observations, and n_o is the number depths being observed, e.g., $n_o = 2$ in this case (temperatures at 5 and 10 cm were assimilated), β is a tuning factor that prevents severe weight degeneracy in the PBS [*Dong et al*., 2016]. As this experimental setup is similar to that used by *Dong et al*. [2016], a value of 0.25 is used for β. If the transition prior distribution is used as the proposal distribution, equation (24) is reduced to

$$w_t^{i*} \propto w_{t-L}^{i*} p(\mathbf{y}_{t-L+1:t} | \mathbf{x}_{t-L+1:t}^i) \tag{26}$$

The normalized weight (w_t^i) is calculated as

$$w_t^i = \frac{w_t^{i*}}{\sum_{i=1}^{N} w_t^{i*}} \tag{27}$$

The resampling method described by *Moradkhani et al*. [2005b] is used in this study. After resampling, all particle weights will be set to $1/N$. A detailed derivation of the PBS algorithm is provided in *Dong et al*. [2016].

Perturbing the estimated parameter set is usually required to avoid parameter impoverishment [*Moradkhani et al*., 2005a,b; *Montzka et al*., 2011]:

$$\mathbf{b}_t^i = \mathbf{b}_t^i + \epsilon_b \tag{28}$$

where ϵ_b is normally distributed noise with zero mean, and standard deviation (Std) of s. In this study, s is determined as follows:

$$s = \max(0, Q_0 - \mathrm{Std}(\mathbf{b}_t)) \tag{29}$$

where Q_0 is a prescribed threshold, which was discussed in *Su et al*. [2011]. The parameter estimates are usually insensitive to Q_0. Using large Q_0 values allows the prior guesses to better encompass the optimal

parameter sets. However, when Q_0 is too large, the prior guesses may contain physically unreasonable combinations of model parameters, which can lead to numerical instability of the forward model. Similar to *Dong et al*. [2016], Q_0 is set to be 10% of the initial parameter standard deviation. This perturbation technique guarantees the parameter distribution has a minimum amount of spread, and this spread cannot grow uncontrollably through perturbation [*Aksoy et al*., 2006].

For the case in which only soil moisture and temperature are updated, *Dong et al*. [2015b] showed that 100 particles are adequate. Jointly estimating soil properties and soil states increases the dimension of the problem and so more particles are required to capture the prior distribution. Synthetic experiments reported by *Dong et al*. [2016] showed that 300 particles were sufficient to estimate model parameters and states. Since the experiment settings and dimension of this study are similar to those of *Dong et al*. [2016], 300 particles are also used here.

2.3. Online Estimation of Observation Depth

In previous studies, it was assumed that the depths of the temperature measurements were perfectly known [*Dong et al*., 2015a,b 2016]. While this is a reasonable assumption for carefully installed point sensors, cable depths in DTS installations can vary considerably due to ground roughness, stones, etc.

Here a version of the PBS algorithm (denoted PBS-D) includes the observation depths as free parameters. The observation depths are randomly sampled from a prior distribution for each particle.

The observation depths are updated jointly with other parameters. Once the observation depths are updated, the measurement operator (h in equation (22)) will be modified to ensure that the simulated observations are at depths consistent with the estimated cable depths.

2.4. Data Collection

The soil temperature and moisture data and soil properties used in this study were collected from the Soil Moisture Active Passive (SMAP) Marena Oklahoma In-Situ Sensor Testbed (MOISST). This is a field site designed for cross-validation of different soil moisture measurement techniques, with the goal of facilitating the validation of remote sensing measurements from SMAP with in situ sensors distributed around the globe [*Cosh et al*., 2010]. The soil moisture and temperature data were collected using Hydra probe (Hydra Probe II, Stevens Water Inc., Portland, OR, USA) from 25 June to 8 October 2010. Data were collected at four sites within a field approximately 0.16 km^2 in area. The soil properties profiles are quite distinct across the four sites (Figure 1).

Hourly soil temperature and moisture data were measured at 2.5, 5, 10, 20, and 50 cm at sites A, B, and D. Site C has similar soil moisture and temperature measurement depths, but the deepest sensor is located at 40 cm. Meteorological forcing data including 5 min precipitation, solar radiation, humidity, air temperature, and wind speed were obtained from the Oklahoma Mesonet site at Marena [*McPherson et al*., 2007].

For real-world experiments, additional soil property data were collected at the four sites for validation. Field capacity (θ_{33}), approximated by the soil water content at a matric potential of -33 kPa, was considered as an indicator of the accuracy of the estimated soil hydraulic properties. Soil thermal properties from 5 to 10 cm were measured at different soil water contents using a dual-probe heat-pulse sensor (KD2Pro, Decagon Devices, Pullman, WA) at sites A, B, and C. The measured soil thermal properties will be used to evaluate the estimated soil thermal conductivity curve.

2.5. Data Assimilation Experiments

First, we quantified the improvement due to the inclusion of the canopy energy balance scheme in the forward model using synthetic tests. Two open loop runs were performed, i.e., the particles were run in parallel without any data assimilation. The open loop for vegetated areas (OL-V) uses Hydrus-V, the version of Hydrus-1D that includes the new canopy energy balance scheme. The open loop for bare soil (OL-B) uses the original Hydrus-1D model. Results from both open loop runs will be compared to a truth generated using Hydrus-V with perturbed parameters and model forcing. Similarly, the PBS scheme will be implemented using both versions of the forward model. PBS-V and PBS-B denote the cases where Hydrus-V and Hydrus-1D are used. Both PBS schemes assimilate synthetic soil temperature observations generated by adding white noise with a standard deviation of 0.5°C to the synthetic true temperatures at 5 and 10 cm. In both PBS schemes, the soil temperature and moisture profiles, soil hydraulic properties (θ_r, θ_s, α, n, and K_s),

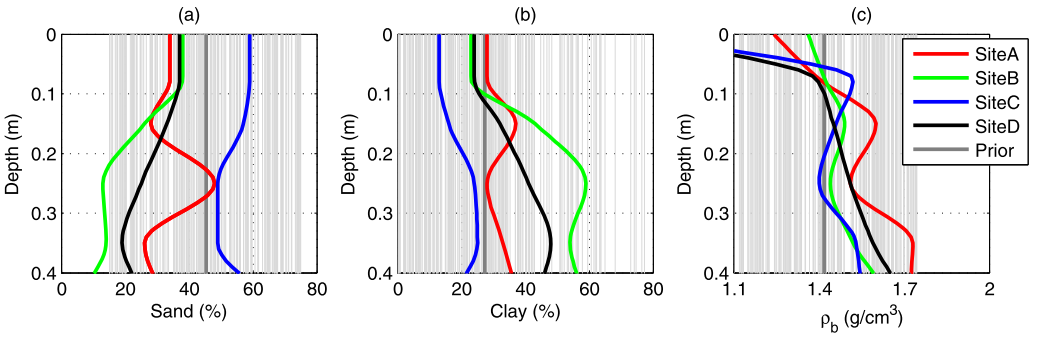

Figure 1. (a, b) The measured soil texture and (c) soil bulk density at different depths. Each thin gray line represents the prior guessed soil texture/bulk density profile for one particle.

and soil thermal property (λ_{sat}) are jointly updated. A priori soil hydraulic properties were generated using ROSETTA [*Schaap et al.*, 2001] with randomly sampled soil texture and bulk density (Table 1). The randomly sampled soil texture and bulk density were also used to provide the initial guesses of the λ_{sat} [*Lu et al.*, 2007] for each particle. In PBS-V, LAI is also estimated. To test the robustness of the approach, this experiment will be repeated 10 times, where each of the 10 synthetic truths are generated using randomly sampled parameters covering a wide range of soil and vegetation properties. Hence, this multiple truths tests will provide more comprehensive comparisons of the performances of the PBS-V and PBS-B.

Next, we will consider the case where the observation depths are not perfectly known. In DTS installations, cable depths can have an uncertainty of a few centimeters [*Steele-Dunne et al.*, 2010]. Hence, it is more realistic to assume that the true cable depth is unknown which means that the a priori mean cable depth may be biased with respect to the truth. In other words, we are interested in whether the PBS can draw the estimated cable depths closer to the truth, even when the initial guesses are biased. In our synthetic experiment, the "true" observation depths are known to be 5 and 10 cm. However, to simulate a scenario where the actual depth is uncertain, the mean of the initial guess for the observation depths was drawn from a uniform distribution between 3 and 7 cm, and 8 and 12 cm, respectively. The standard deviation of the initial guess is assumed to be 1 cm. This extension of the PBS-V, in which the observation depths are also estimated, will be denoted "PBS-D." In synthetic tests, using the same 10 truths as before, the PBS-D algorithm will be benchmarked against the PBS-V. Finally, the PBS-D algorithm will be tested using real-world data from four observed soil temperature and moisture profiles at the SMAP MOISST site.

3. Results and Discussion

3.1. The Canopy Energy Balance Scheme

Figure 2 shows an illustrative case that compares the estimated soil moisture using the OL-V, PBS-V, and PBS-B. From 2.5 to 20 cm deep, the estimated soil moisture from the PBS-B is (dry) biased compared to the truth. In the PBS-V estimates, the large errors in initial conditions persist for a few days, but the PBS-V tracks the truth accurately from 1 July to the end of the simulation period. The soil moisture at 50 cm from the PBS-V is significantly wetter than the truth and is worse than both the OL-V and PBS-B. This is because only surface soil temperatures (5 and 10 cm) were assimilated, and these temperatures contain little information

Table 1. Generation of Perturbed Inputs (Soil and Vegetation Property and Forcing) for Each Particle

Variable	Error Distribution	Mean	Std.	Bound
Sand (%)	Uniform			15, 75
Silt (%)	Uniform			0, 100 - Sand
ρ_b (g/cm^3)	Uniform			1.1, 1.7
Air temperature (°C)	Gaussian, additive	0	+0.5	
Precipitation (mm)	Gaussian, multiplicative	1	×0.2	
Radiation (W/m^2)	Gaussian, multiplicative	1	×0.075	–, 1350
Relative humidity (%)	Gaussian, multiplicative	1	×0.05	–, 100
Wind speed (km/h)	Gaussian, multiplicative	1	×0.2	
Vegetation parameters	Gaussian, multiplicative	1	×0.2	

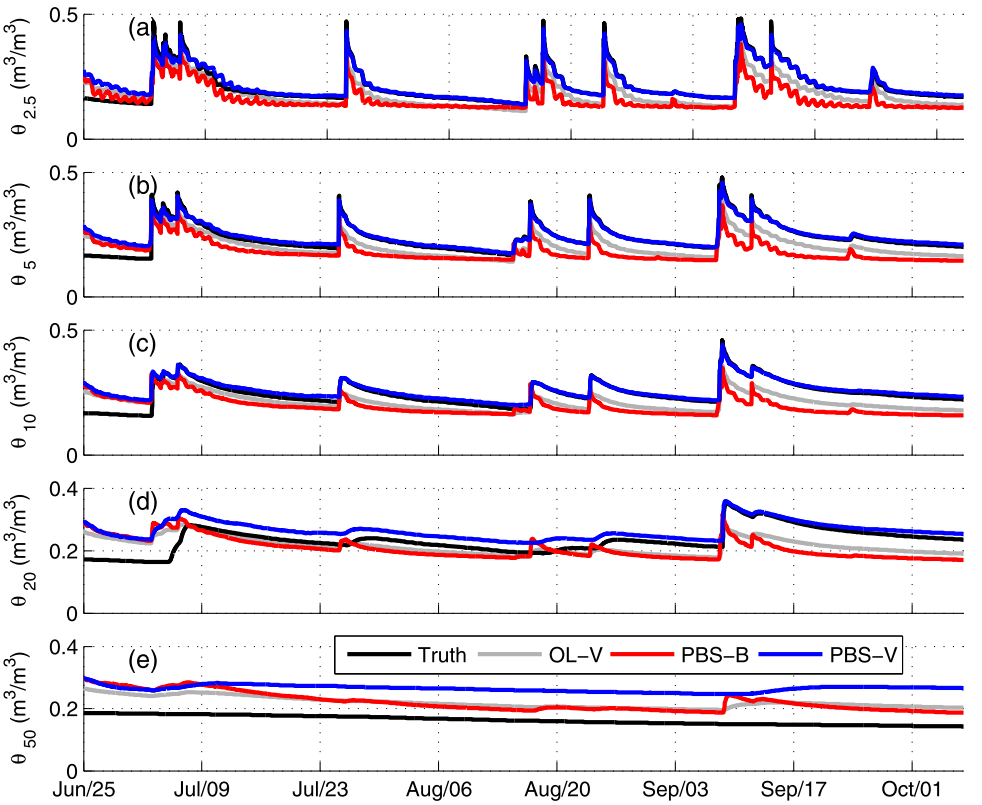

Figure 2. Comparison of soil moisture estimated using different approaches at five depths.

on soil moisture at 50 cm [*Dong et al*., 2015a]. Furthermore, as the soil moisture at depth has little response to meteorological forcing during this time period (Figure 2e), the soil moisture at depth is not correlated with shallow soil moisture. Under these conditions, the primary impact of assimilating surface soil temperatures on the soil moisture at depths is through model physics [*Dong et al*., 2015a], i.e., by adding or extracting water at surface layers the PBS will draw the deeper layers toward a wetter or drier condition. In this specific case, the true soil moisture is wetter than the OL-V at the surface and drier than the OL-V at 50 cm. The PBS-V corrects the estimates from 2.5 to 20 cm toward a wetter condition, which leads to a higher (incorrect) soil moisture at 50 cm. The bias at depth (e.g., Figure 2e) is largely an uncorrected bias in the prior initial condition. In Figures 2a–2e, the OL-V, PBS-B, and PBS-V all start with the same prior initial condition, i.e., initial soil moisture and temperature are assumed to be homogeneous with depth, and the values randomly sampled from U [0.15 m^3/m^3, 0.4 m^3/m^3] and U[20°C, 40°C] for soil moisture and temperature, respectively. It is clear from Figure 2a that assimilation of temperature observations and the impact of precipitation in "reinitializing" surface soil moisture are both effective in removing this initial bias at the surface. The degree to which this occurs decreases with depth (see Figures 2b–2e). The root zone soil moisture has little correlation to the surface soil moisture, and little response to meteorological forcing. Hence, as shown by *Dong et al*. [2015a], the error in the prior guessed root zone soil moisture is difficult to correct using the soil temperatures from the shallow subsurface. As shown in Figure 2d, the bias persists for approximately 4–5 weeks at 20 cm, until the soil moisture is gradually drawn to the truth at the end of the simulation. At 50 cm, it persists beyond the simulation period. The estimated soil moisture, particularly at depth, could be improved by employing bias correction methods analogous to those employed by *Ryu et al*. [2009], *De Lannoy et al*. [2007], *Dee and Da Silva* [1998], and *Monsivais-Huertero et al*. [2016].

The soil hydraulic properties estimated using the PBS-B and PBS-V in this illustrative case are shown in Figure 3. The θ_r and α estimates in the PBS-B converge to the truth during the simulation period. However, the PBS-B draws the estimated n and K_s toward a wrong value, which is significantly worse than the prior guess. As a result, the estimated soil water retention curve is significantly biased compared to the truth (Figure 3h). The

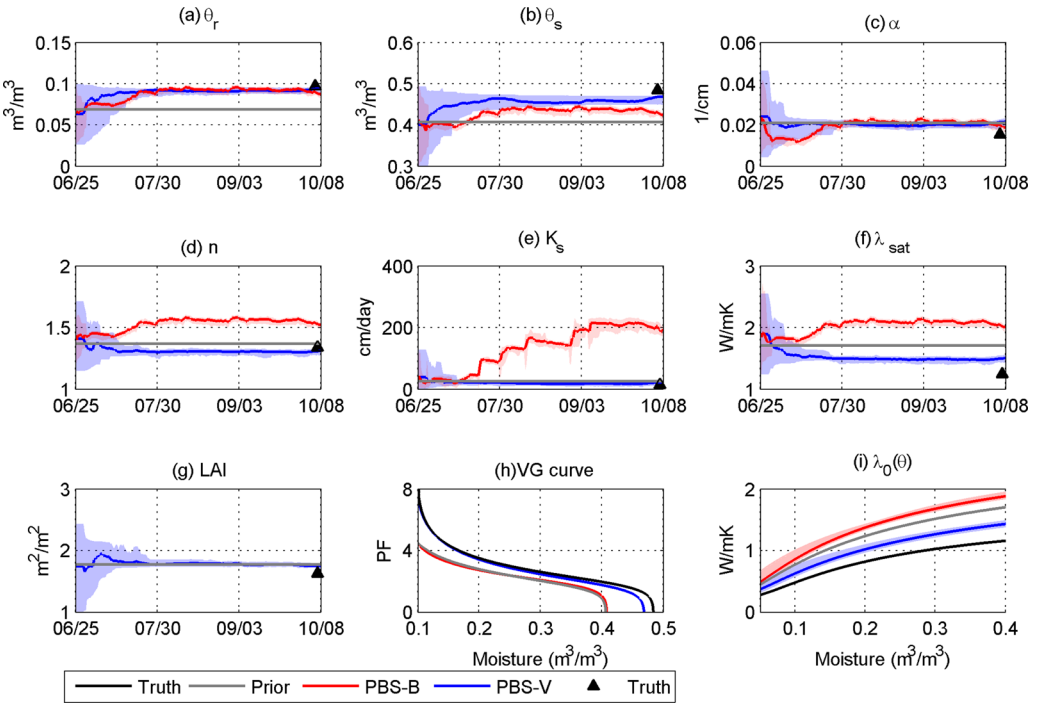

Figure 3. The convergence of (a–e) the estimated soil hydraulic properties, (f) λ_{sat}, (g) LAI and (h) the soil water retention curve and (i) the thermal conductivity curve using the estimated soil hydraulic and thermal parameters.

estimated soil hydraulic parameters from the PBS-V all converge to the true values after a few updates. The estimates are nearly constant during the entire simulation period, which means the estimates are accurate and robust. Because the parameters are correct, the soil water retention curve from the PBS-V fits the truth accurately (Figure 3h). In this specific case, the true LAI is quite close to the mean of the prior guess. Hence, little improvement is shown in the mean of the PBS-V estimates compared to the prior guess. For the thermal properties, the estimated λ_{sat} is shown in Figure 3f. Similar to the soil hydraulic properties, the PBS-B provides an even worse estimate than the prior guess. The PBS-V quickly draws the initial guess closer to the truth, which results in an improved soil thermal conductivity curve (Figure 3i). Consistent with a previous study [*Dong et al.*, 2016], the soil thermal conductivity curve is more difficult to estimate with this approach than the water retention curve. This is because the soil hydraulic properties, through their impact on variations in soil moisture, are the dominant control on soil temperature dynamics.

Box plots comparing the open loop and PBS soil moisture estimates for the 10 synthetic truths are given in Figure 4. The median RMSE of soil moisture estimates using OL-V constantly is smaller than that estimated using OL-B at all depths. In general, the differences between OL-B and OL-V increase with depth. This is because the OL-B ignores the root water uptake processes in the root zone. The increased interquartile range (IQR) of the RMSE of the PBS-B estimated soil moisture indicates that the PBS-B can be even worse than the OL-B for some cases.

When the canopy energy balance scheme is included in the forward model (PBS-V), the soil moisture can be robustly estimated across the entire profile, with RMSE values often <0.02 m^3 m^{-3}. It is shown that the performance of the PBS-B significantly depends on the temporal mean of the truth. Figure 4f shows the difference between the RMSE of soil moisture estimated using PBS-B and PBS-V at 5 cm as a function of true soil moisture. In general, when the temporal mean of the true soil moisture is low, the performance of the PBS-B and PBS-V is comparable. However, when the temporal mean of the truth is high, using PBS-B yields significantly degraded soil moisture estimates compared to the PBS-V.

This can be explained by the fact that soil heat and water transfer processes are more tightly coupled under dry soils. Soil heat transfer strongly depends on soil moisture when soil moisture is low [*Steele-Dunne et al.*, 2010]. Hence, heat transfer processes between two depths (i.e., 5 and 10 cm) contain more information about soil moisture when the soil is dry. Furthermore, the energy lost through evaporative cooling is

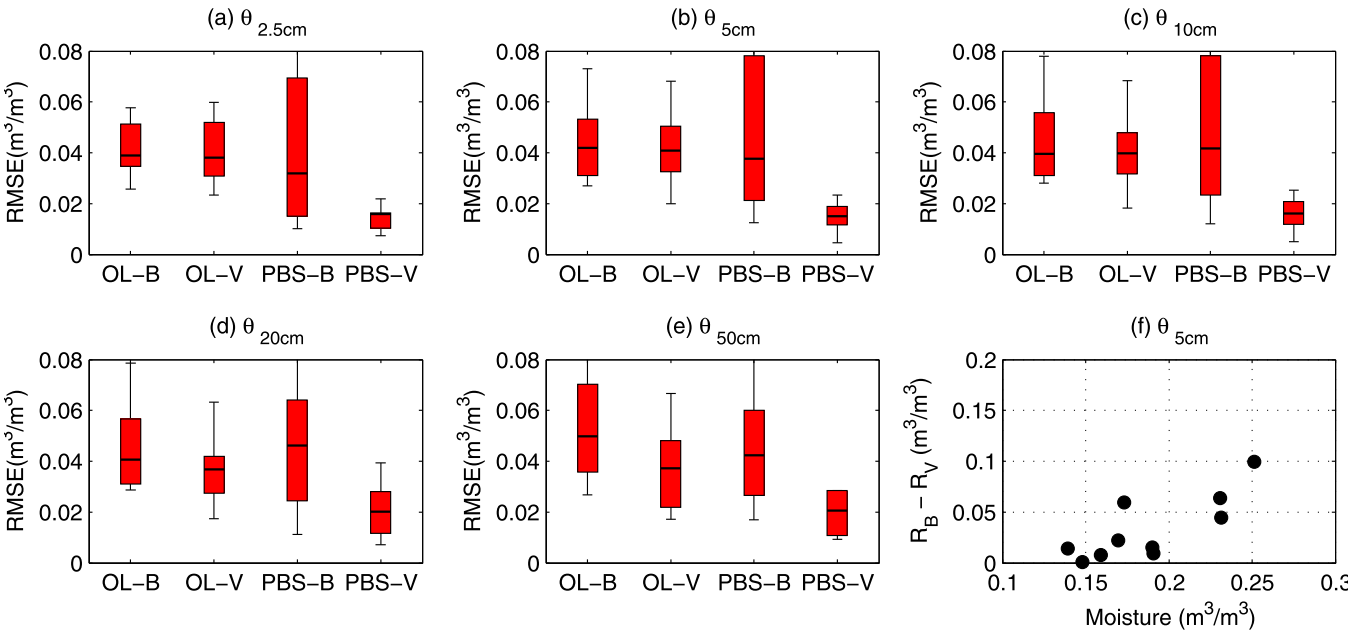

Figure 4. (a–e) The RMSE of soil moisture estimates using four different approaches at five depths and (f) the differences of the RMSE of the PBS-B and PBS-V estimated 5 cm soil moisture as a function of the temporal mean of the true soil moisture at 5 cm. Each box plot contains results derived from synthetic tests using 10 randomly selected truths.

primarily controlled by the availability of soil moisture under dry soils. This means the cooling/heating rate of the soil is a strong function of soil moisture. When the truth is dry, soil moisture can be relatively well estimated using soil temperatures, even though the forward model has large structural errors (e.g., PBS-B).

The estimated model parameters are compared to the synthetic "true" values in Figure 5 and Table 2. As expected, the estimated parameters from the PBS-V are closer to the 1:1 line than those estimated using PBS-B. Several parameters estimated using the PBS-B are even negatively correlated to the truth (Table 2). The large errors in estimated θ_{33} (Figure 5g) from the PBS-B imply a poor agreement between the estimated and true soil water retention curves.

In the PBS-V, α and K_s are relatively poorly estimated. However, the other parameters suffice to ensure that the θ_{33} is well estimated (Figure 5g and Table 2), and hence that the estimated and true water retention curves are similar.

LAI determines canopy extinction of the net radiation, which influences the amplitude of the simulated soil temperatures. Hence, LAI can be accurately inferred from the soil temperature observations using PBS-V (Figure 5h).

3.2. State-Parameter Estimation With Unknown Observation Depths

The illustrative case is revisited in Figures 6a and 6b which show the estimated sensor (observation) depths using PBS-D. In this case, the prior guess for the depths is 4.3 and 10.7 cm. For the top sensor, the PBS-D converges to the true sensor depth after a few updates. Though the estimated depth lower sensor is closer to the true value than the prior, it is still 0.5 cm from of the true value by the final time step. Once the estimated depths converge from the highly uncertain initial guess, the estimates of the depths remain constant. The reduction of the uncertainties in the sensor depths is also quite noticeable.

Figure 6c shows box plots of the errors in estimated cable depths for 10 different truths. The median error of the estimated cable depth is approximately 0.3 cm for the top sensor depth, and 0.5 cm for the lower sensor depth. The amplitude of the temperature wave induced by the diurnal cycle of solar radiation is damped with increasing depth [*Steele-Dunne et al.*, 2010; *Arya*, 2001]. As a result, the error in the estimated lower sensor depth may reach up to 1.2 cm, which is significantly larger than that of the top cable. It is more challenging to correct the initial errors of the lower cable (Figure 6d). This is because the solar signals

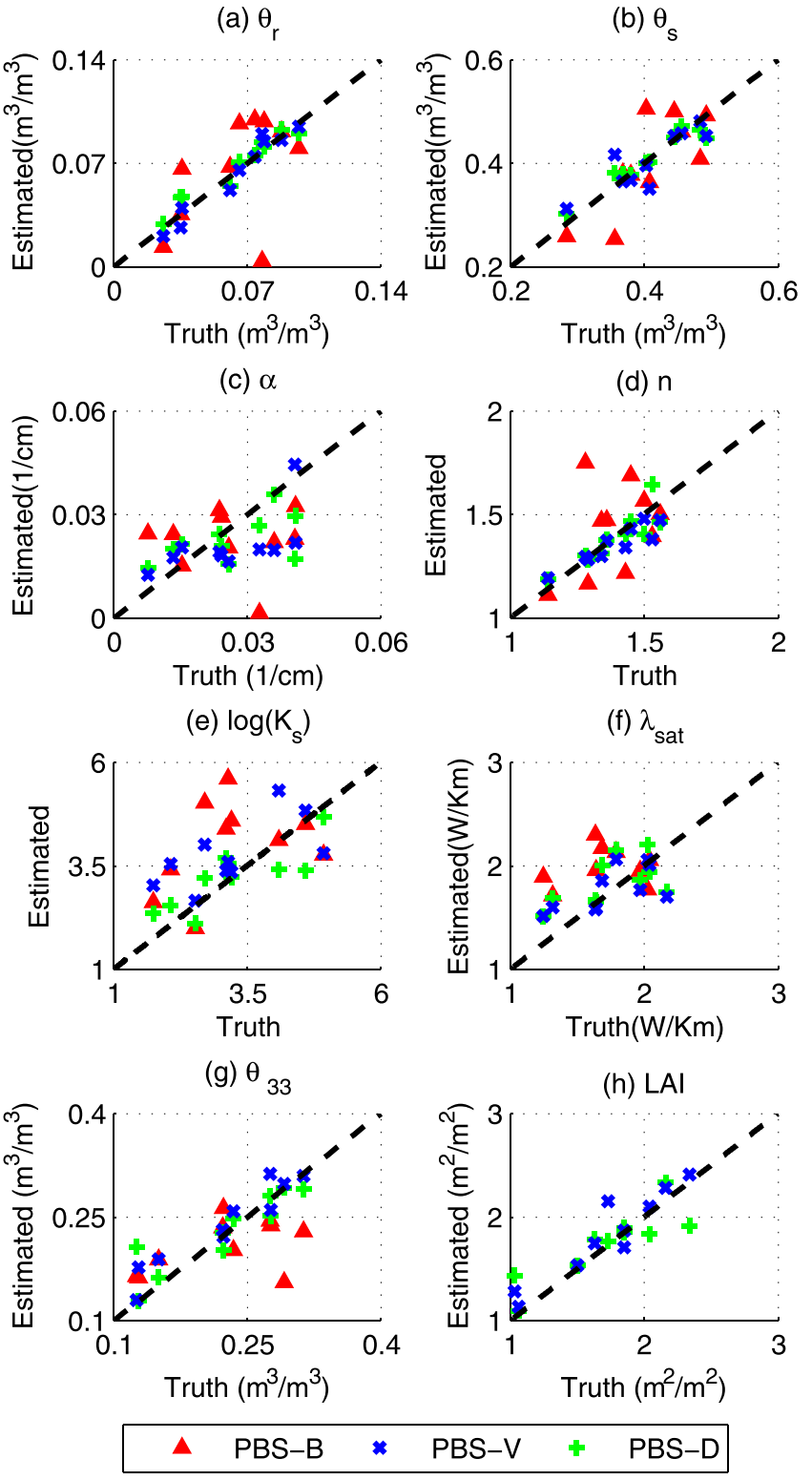

Figure 5. Comparison of (a–e) the estimated soil hydraulic properties, (f) λ_{sat}, (g) θ_{33}, and (h) LAI using three different PBS strategies.

decrease exponentially with depth. Hence, little information is available to estimate the cable depth of the lower cable. As for the upper cable, the depth can be well estimated regardless of whether the prior guess is positively or negatively biased with respect to the truth.

Table 2. Correlation Coefficient of the Estimated and the True Parameters Using Three Different Data Assimilation Approaches[a]

Par.	PBS-B	PBS-V	PBS-D
θ_r	0.51	0.97	0.97
θ_s	0.77	0.86	0.96
α	−0.01	0.61	0.55
n	0.39	0.91	0.88
K_s	−0.09	0.42	0.82
λ_{sat}	−0.38	0.63	0.57
θ_{33}	0.49	0.95	0.90
LAI		0.87	0.94

[a]The values are calculated using the estimates from 10 randomly selected truths.

The parameters estimated using PBS-D can be compared to those from PBS-V in Figure 5 and Table 2. In general, the PBS-D provides very similar results to the PBS-V. Consequently, the accuracy of the soil moisture estimates using the PBS-V and the PBS-D are also quite similar (Table 3). At 2.5–20 cm, the maximum difference in RMSE is just 0.03 m^3/m^3. The similar performance of PBS-D and PBS-V is remarkable given that the sensor depths are perfectly known in PBS-V, and unknown but estimated in PBS-D. This means that in DTS applications, the PBS-D can be used to estimate soil moisture even when there is significant uncertainty in the cable depths.

3.3. Real Data Application

The PBS-D algorithm was applied to four real, observed soil temperature profiles at the SMAP MOISST site. First, the error of the estimated sensor depths for the four sites is shown in Table 4, and the convergence of the estimated sensor depths at sites A and C is shown in Figure 7. The initial/prior sensor depths at site A are approximately 2 cm biased for both the upper and the lower sensors (Figures 7a and 7b). The PBS-D draws the estimates to the observed sensor depths, and the error of the final estimates is 0.15 and 0.69 cm for the upper and lower sensor, respectively. The uncertainties of the sensor depths are considerably reduced. The same prior sensor depths were assumed for site C, and again they are biased with respect to

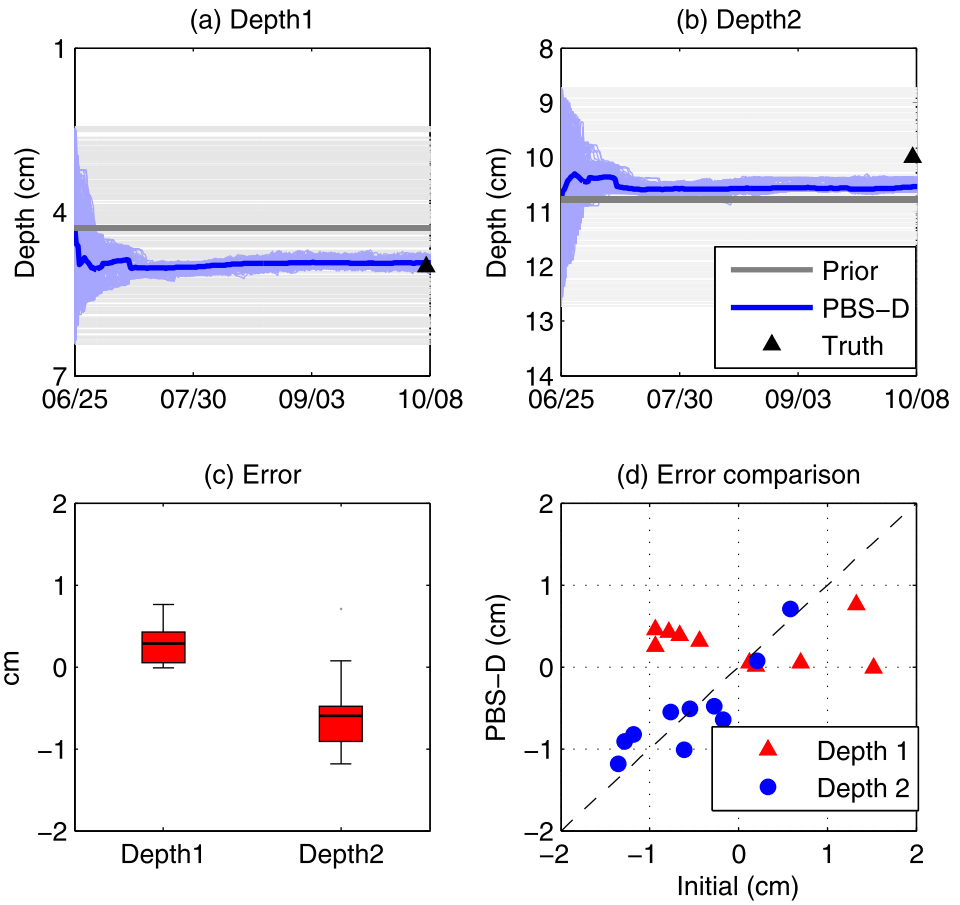

Figure 6. The convergence of (a, b) the two estimated observation depths in one illustrative example, (c) the error of the estimated observation depths tested by 10 randomly selected truths, and (d) a comparison of the PBS-D and the prior guessed cable depths error. In Figure 6a and 6b, each thin line represents one particle. The true observation depth is shown at the final estimation step.

Table 3. The RMSE of Soil Moisture Estimates (m^3/m^3) at Five Depths Using the PBS-V and the PBS-D[a]

	Depth				
	2.5 cm	5 cm	10 cm	20 cm	50 cm
PBS-V	0.013	0.015	0.016	0.018	0.025
PBS-D	0.016	0.017	0.018	0.021	0.031

[a]The RMSEs are averaged from 10 randomly selected truths.

the measured values. It takes longer for the PBS-D estimate of the top sensor depth to converge. When it does, the estimate is closer to the truth but still has an error of 0.66 and 1.58 cm for the upper and lower sensor (Table 4). Similar to the synthetic tests, estimates for the lower sensor are less robust (Table 4). As discussed in the previous section, the signal from solar radiation is damped exponentially with depth. In addition, the time lag in the propagated soil temperature fluctuations also increases with depth. Hence, soil temperature contains less information of the observation depths for the lower sensor.

Figure 8 illustrates the convergence of the estimated model parameters using sites A and C as illustration. The estimated θ_r, θ_s, and α converged to similar values at the two sites. However, the PBS-D estimates show that site C has a significantly larger n and K_s. The sand content of site C is approximately 22% higher than that of site A on average (Figure 1). Saturated soil hydraulic conductivity and the van Genuchten parameter n typically increase with sand content [*Rawls et al.*, 1982]. This suggests that the differences in estimated K_s and n between the two sites are reasonable. The estimated θ_{33} based on the estimated soil hydraulic properties at the two sites is shown in Figure 8f. The PBS-D draws the estimated θ_{33} closer to the observed value at site A. At site C, the θ_{33} seems to be slightly overfitted, i.e., the value from PBS-D is further from the observed value than the prior guess. Another parameter that clearly shows the difference between the two sites is λ_{sat}. This leads to different estimated soil thermal conductivity curves at the two sites, both of which are closer to the observations (Figure 8i) than the prior. The evolution of the estimated parameters is slightly more variable than in the synthetic tests (Figure 3). This may be due to increased model structural errors in the real-world application. For example, the forward model assumes the soil property profile is uniform, which is not true in reality (Figure 1).

In Figures 9 and 10, results are compared from the OL-V and PBS-D to show the benefit of assimilation in a real DTS application. The forward model is the same in both OL-V and PBS-D. The PBS-V and PBS-B are not included here as they require that the cable depths are perfectly known. The estimated soil moisture at site A is shown in Figure 9. Compared with the OL-V, the main benefit of assimilating soil temperatures is between the surface and 10 cm deep, i.e., the depth of the deepest soil temperature observation. The reduction in RMSE at shallow depths is significant (Figure 9a and 9b and Table 5). By adjusting the shallow soil moisture to a wetter condition, the soil moisture estimates at 20 and 50 cm were also improved through the model. Similar findings were also shown in the estimates of sites B and D in the supporting information.

At site C, the OL-V provides reasonable estimates of soil moisture at all depths, despite the large particle ranges (Figure 10). The PBS-D provides further improvement at depths from 5 to 40 cm. In general, the largest errors in PBS-D estimated soil moisture occur in the first week of the simulation (i.e., before 9 July). This is because soil temperature and not soil moisture is assimilated, and so the PBS-D adjusts the soil moisture to compensate for errors in the initial guessed model states and parameters.

In general, the largest RMSE of the soil moisture estimates at depths above 10 cm is approximately 0.04 m^3/m^3 (Table 5). Improvements below 20 cm are primarily through model physics. Improving soil moisture estimates at shallow depths will eventually lead to improved root zone soil moisture estimates. However, this means errors in the initial deep soil moisture persist for a few months, since the correlation between the surface and deep soil moisture is relative low and there are limited dynamics below 20 cm. Table 5 shows the RMSE in the estimated soil moisture at all depths, at sites A–D. From the surface to a depth of 10 cm, most RMSE values are around 0.02–0.04 m^3/m^3, which is comparable in magnitude to the measurement error associated with the "ground truth" soil moisture probe. Consistent with the synthetic tests, the best assimilation results are obtained in the top 10 cm, i.e., at and above the cable depths. At depths greater than 20 cm, the impact of solar radiation is reduced so there is limited variation in temperature and therefore little correlation with the temperatures observed and simulated closer to the surface. Assimilation therefore leads to a limited improvement at depth due to the

Table 4. The Absolute Error (cm) of the Estimated Sensor Depths at the Four Sites

	Prior	Site A	Site B	Site C	Site D
Depth 1	2.117	0.153	0.086	0.659	0.413
Depth 2	1.954	0.698	0.027	1.578	0.255

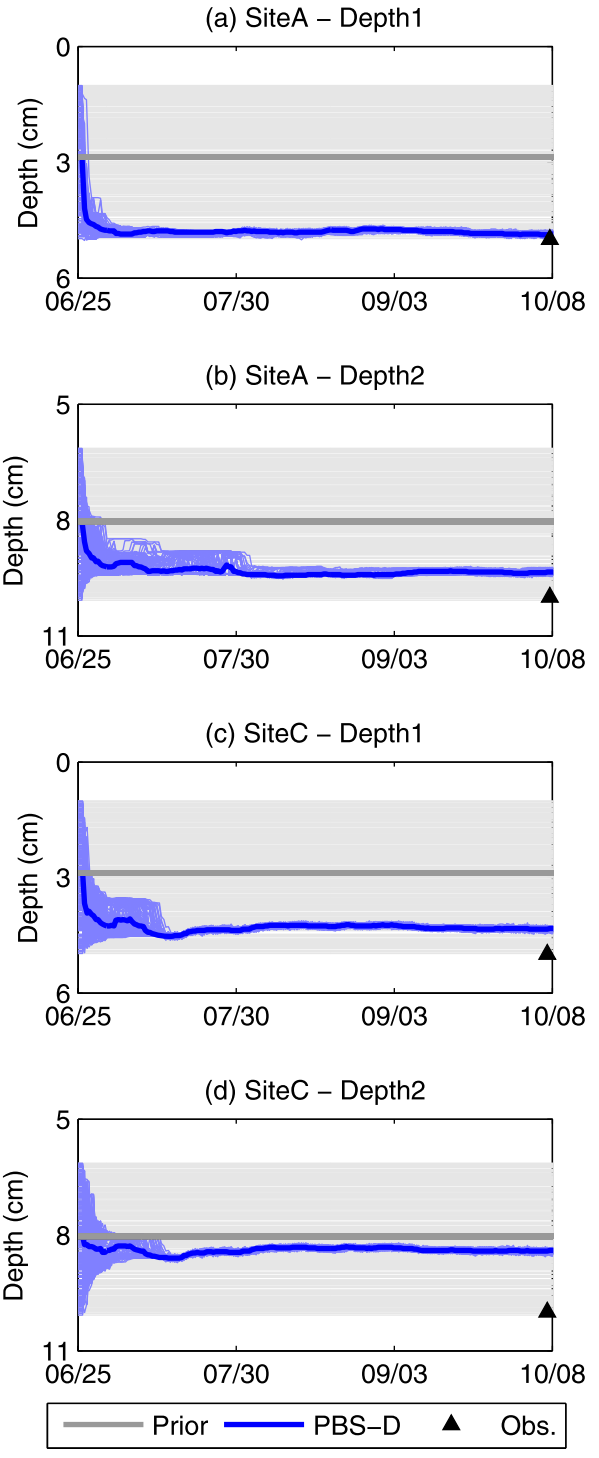

Figure 7. The convergence of the estimated sensor depths at (a, b) site A and (c, d) site C. The observed sensor depth is shown at the final time step of the simulation.

persistence of bias from the initial condition. With the exception of site C, the RMSE from PBS-V is lower than that from OL-V, confirming that assimilation generally leads to an improvement over the open loop. At site C, the OL-V yields RMSE values that are comparable to the measurement error of the soil moisture probe at site C. Though assimilation appears to worsen the estimate, the magnitude of these errors means that the estimates have essentially the same accuracies. The value of including the vegetation scheme is clear from the reduction in RMSE when PBS-V is used instead of PBS-B. The reduction of RMSE is typically around 20–30%. The most important result, in the context of applying this approach to a real DTS application, is that the PBS-D performance is very similar to that of PBS-V. Recall that PBS-V and PBS-D are identical in terms of model physics. The only difference is that the cable depths are unknown in PBS-D and are included with the parameters to be estimated. Though the performance of the PBS-V is excellent, its value is limited by the need to know the cable depths. The fact that the PBS can estimate these depths and yield comparable performance when the cable depths are unknown removes the final barrier to applying the PBS approach to real DTS data. Finally, it is noteworthy that the relative performance of the PBS implementations is consistent with that observed in the synthetic experiments.

Figure 11 further demonstrates the potential of using soil temperature observations to detect the spatial variability of soil moisture and soil properties. The OL-V uses the same a priori model parameters and forcing data, and hence it provides the same estimates across all the four sites, i.e., no soil moisture or soil property difference can be detected by the OL-V. The temporal mean soil moisture is most accurately estimated by PBS-D at the depth of 2.5 cm. It correctly shows that site C is drier than the other three sites. Also, sites A, B, and D have similar temporal mean soil moisture. The accuracy of the PBS-D estimates decreases with increasing depth and is significantly biased at sites A, B, and D at 20 cm. The variability of the temporal mean soil moisture across the four sites is still well captured. Similar to the soil moisture estimates, the PBS-D correctly shows the variability of the θ_{33} across the four sites using soil temperature dynamics. The estimated θ_{33} at sites B–D are slightly biased (0.037 m^3/m^3 at sites B and D and 0.044 m^3/m^3 for site C). However, given the accuracy of the field measured θ_{33}, the PBS-D estimates are quite acceptable. PBS-V generally provides

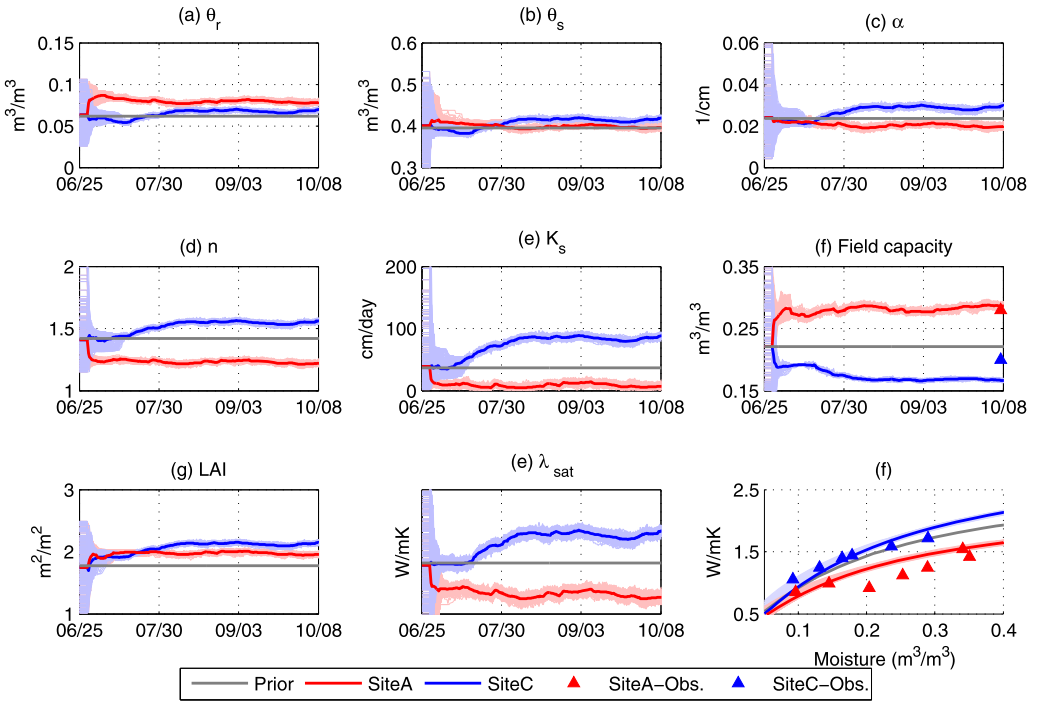

Figure 8. The convergence of (a–e) the soil hydraulic properties at site A and site C, (d) LAI, (f) a comparison of the PBS-D estimated and the observed θ_{33} and (i) the soil thermal conductivity curve.

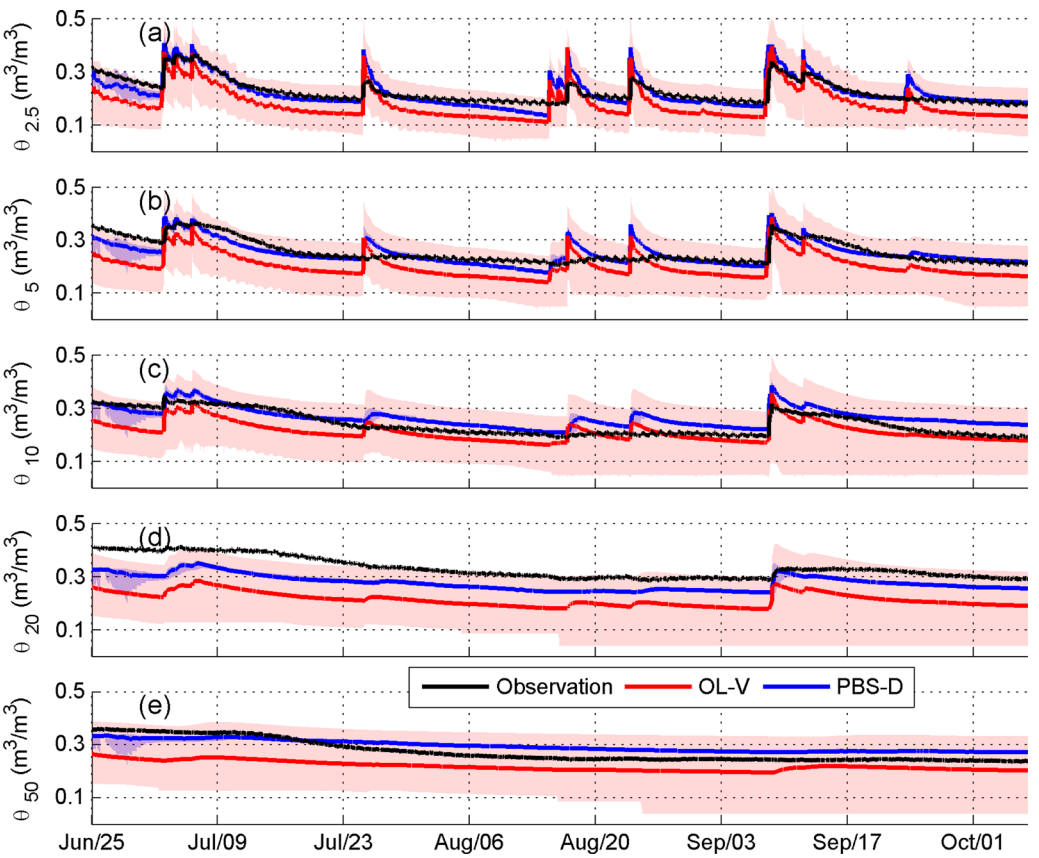

Figure 9. Comparison of estimated soil moisture using PBS-D and OL-V at five depths at site A. The shaded area represents the range of the particles.

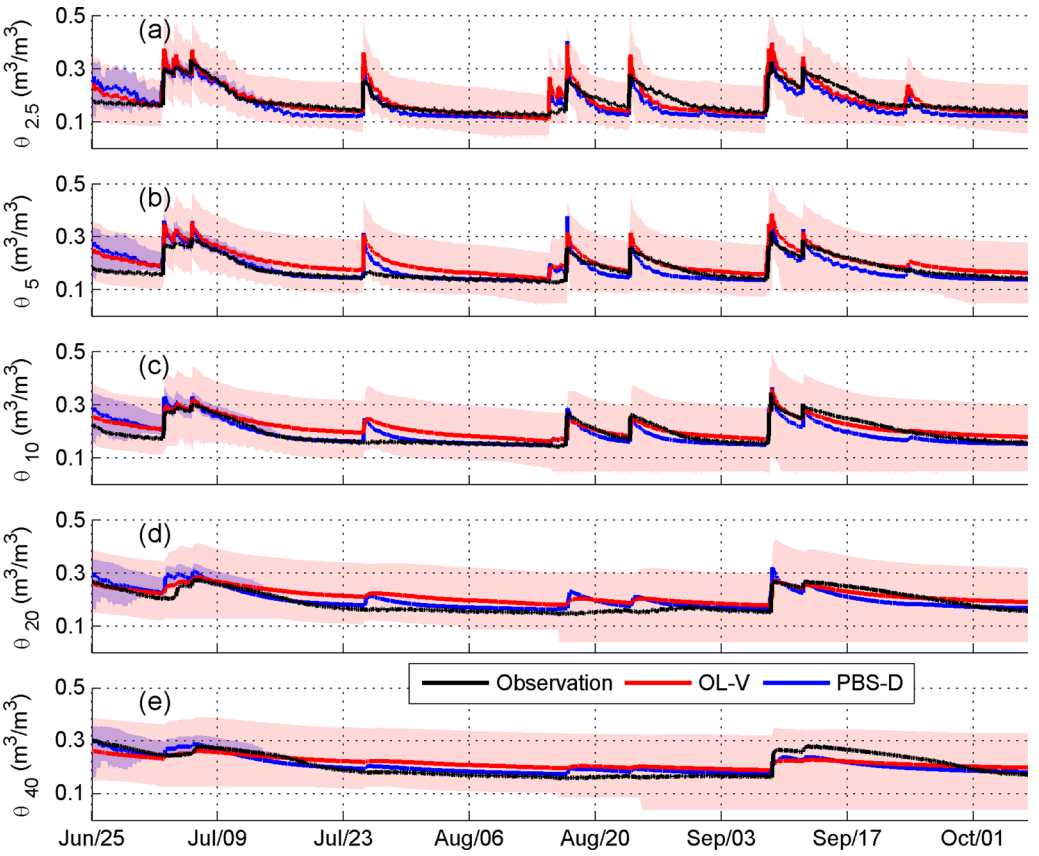

Figure 10. Similar to Figure 9, but for site C.

similar results to PBS-D, which is consistent with the synthetic test. The PBS-B can also be reasonably estimated the mean soil moisture and the θ_{33} across the four sites. This may demonstrate the feasibility and robustness of using soil temperatures from DTS for high-resolution soil moisture mapping.

4. Conclusions

In this study, we solved the two key remaining barriers to the application of Passive DTS for large-scale high-resolution soil moisture monitoring. First, the inclusion of a new surface energy balance scheme in the

Table 5. The RMSE of Soil Moisture Estimates (m^3/m^3) at Five Depths Using the OL-V and the PBS-D at Four Sites[a]

Sites	Appro.	2.5 cm	5 cm	10 cm	20 cm	40/50 cm
A	OL-V	0.053	0.060	0.039	0.074	0.037
	PBS-V	0.034	0.040	0.040	0.057	0.030
	PBS-D	0.027	0.026	0.034	0.057	0.030
	PBS-B	0.046	0.051	0.058	0.106	0.092
B	OL-V	0.055	0.026	0.056	0.115	0.159
	PBS-V	0.041	0.035	0.036	0.095	0.127
	PBS-D	0.041	0.030	0.041	0.114	0.140
	PBS-B	0.050	0.050	0.046	0.093	0.138
C	OL-V	0.023	0.031	0.027	0.032	0.035
	PBS-V	0.028	0.034	0.029	0.040	0.038
	PBS-D	0.030	0.027	0.025	0.025	0.023
	PBS-B	0.041	0.024	0.024	0.026	0.027
D	OL-V	0.056	0.058	0.066	0.092	0.153
	PBS-V	0.026	0.029	0.030	0.044	0.093
	PBS-D	0.032	0.031	0.034	0.061	0.111
	PBS-B	0.047	0.046	0.045	0.081	0.184

[a]The deepest measurement and estimated soil moisture depth being compared is 50 cm for sites A, B, and D, and 40 cm for site C.

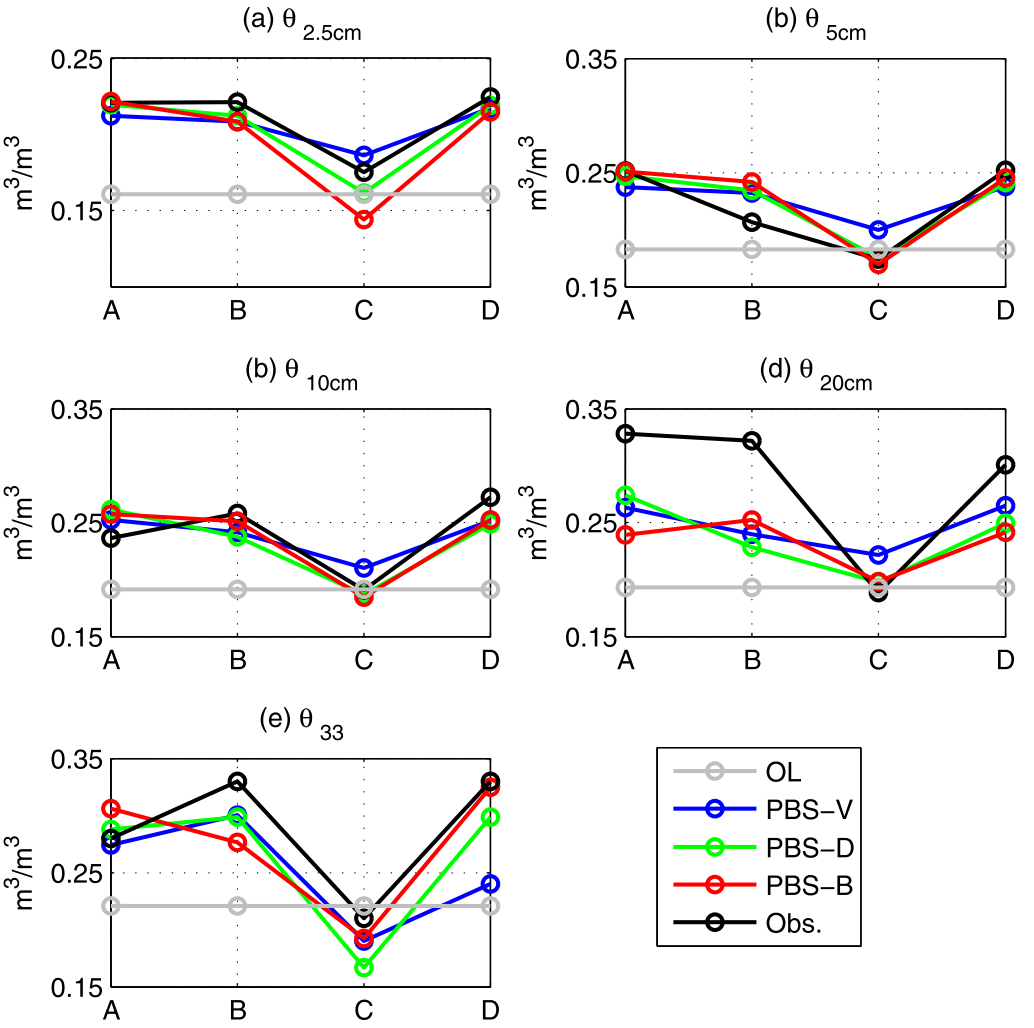

Figure 11. Comparison of (a–d) the estimated and observed temporal mean soil moisture and (e) the θ_{33} at the four sites.

Hydrus-1D model extends the applicability of the PBS data assimilation approach to vegetated areas. This is an essential development to enable the use of Passive DTS for soil hydrology research, and the validation of remote sensing observations under agricultural and natural vegetation. Second, an algorithm was proposed to estimate observation depths jointly with other model states and parameters. This is particularly relevant for DTS applications, since measuring the cable depths every meter along the DTS cable is logistically impractical. Requiring the cable depths to be measured everywhere would render the data assimilation scheme proposed by *Dong et al*. [2015a,b 2016] useless in DTS applications. Therefore, estimating the cable depths is essential.

The new approach (PBS-D) was tested using both synthetic and real-world data. The synthetic experiments were necessary because in real DTS installations, the cable depth is difficult to measure and therefore often unknown. Synthetic tests, in which the cable depth is perfectly known, were used to demonstrate that the proposed approach worked and to illustrate the value of being able to estimate the observation depth. The "real" data were from four observation profiles from traditional sensors rather than DTS observations. These profiles had very distinct soil texture profiles. Though the prior guesses for sensor depths, soil moisture, and properties were identical for all profiles, the PBS-D approach was able to reproduce observed differences in soil properties and soil moisture between the four sites. Hence, the results demonstrate that the PBS-D can be used to assimilate in situ soil temperature observations to simultaneously estimate soil moisture dynamics along with soil hydraulic and thermal properties. It is worth nothing that the cable depths could be calibrated off-line if they are time-invariant parameters. This would reduce the degree of freedom of the estimation problem, potentially improving the estimates of the remaining states and parameters. However,

the ability to estimate them is limited by the uncertainty and/or biases in the soil properties in the prior guess. This would require an iterative procedure to allow both to converge.

This study was motivated by the potential use of DTS observed soil temperatures for submeter scale soil moisture estimation in fiber-optic cables up to kilometers in length. Applying the approach presented here to DTS data means that instead of four profiles, there are thousands whose soil properties are unknown. The results presented here suggest that the PBS-D approach can be used to detect variations in soil properties and soil moisture across all the locations along the cable. This will be used to improve our knowledge about soil moisture scaling between point and intermediate scales, high-resolution soil properties and moisture mapping, and other related research areas. It is particularly important for bridging the observation gap between point sensors and the satellite footprint scale.

Future research will focus on the integration of Active DTS into the PBS-D approach. Active DTS is a more direct way of measuring soil moisture and may be particularly useful when net radiation is low or the estimate uncertainty becomes very high. Smart strategies of combining Active and Passive DTS methods may yield more robust soil moisture and property estimates at intermediate scales. In addition, including more sophisticated parameter perturbation techniques (e.g., Variable Variance Multiplier, VVM approach) [*Leisenring and Moradkhani*, 2012], MCMC algorithms [e.g., *Yan et al*., 2015; *Vrugt et al*., 2013; *Moradkhani et al*., 2012] may further improve the accuracy and the robustness of the presented algorithm.

Acknowledgments
The authors thank Oklahoma Mesonet and Michael Cosh, USDA-ARS Beltsville, MD, for providing model forcing and soil property data. Data used in the present study may be accessed by contacting T. E. Ochsner and M. H. Cosh. The first author was financially supported for his PhD research by the China Scholarship Council with the project reference number of 201206040043. The work of S. C. Steele-Dunne was supported by The Netherlands Organisation for Scientific Research (NWO) Veni Grant Program (ALW 863.09.015). The contribution of T. E. Ochsner was funded by the Oklahoma Agricultural Experiment Station. The SMAP MOISST site was made possible by contributions from the USDA-ARS Hydrology and Remote Sensing Laboratory, Beltsville, MD, and from NASA. The creation of the MOISST site was initiated by M. H. Cosh, and the site is maintained by C. Stansberry and the Oklahoma State University Range Research Station.

References

Aksoy, A., F. Zhang, and J. W. Nielsen-Gammon (2006), Ensemble-based simultaneous state and parameter estimation in a two-dimensional sea-breeze model, *Mont. Weather Rev.*, *134*(10), 2951–2970, doi:10.1175/MWR3224.1.

Arya, P. S. (2001), *Introduction to Micrometeorology*, vol. 79, pp. 41–60, Academic Press, Inc., N. Y.

Bateni, S., and D. Entekhabi (2012), Surface heat flux estimation with the ensemble Kalman smoother: Joint estimation of state and parameters, *Water Resour. Res.*, *48*, W08521, doi:10.1029/2011WR011542.

Bonan, G. B. (1996), A land surface model (LSM version 1.0) for ecological, hydrological, and atmospheric studies: Technical description and user's guide, NCAR Technical Note NCAR/TN-417+STR, National Center for Atmospheric Research, pp. 1–150.

Boni, G., F. Castelli, and D. Entekhabi (2001), Sampling strategies and assimilation of ground temperature for the estimation of surface energy balance components, *IEEE Trans. Geosci. Remote Sens.*, *39*(1), 165–172, doi:10.1109/36.898678.

Caparrini, F., F. Castelli, and D. Entekhabi (2003), Mapping of land-atmosphere heat fluxes and surface parameters with remote sensing data, *Boundary Layer Meteorol.*, *107*(3), 605–633, doi:10.1023/A:1022821718791.

Ciocca, F., I. Lunati, N. Van de Giesen, and M. B. Parlange (2012), Heated optical fiber for distributed soil-moisture measurements: A lysimeter experiment, *Vadose Zone J.*, *11*(4), doi:10.2136/vzj2011.0199.

Clark, M. P., D. E. Rupp, R. A. Woods, X. Zheng, R. P. Ibbitt, A. G. Slater, J. Schmidt, and M. J. Uddstrom (2008), Hydrological data assimilation with the ensemble Kalman filter: Use of streamflow observations to update states in a distributed hydrological model, *Adv. Water Resour.*, *31*(10), 1309–1324, doi:10.1016/j.advwatres.2008.06.005.

Cosh, M. H., T. Ochsner, J. Basara, and T. J. Jackson (2010), The SMAP in situ soil moisture sensor testbed: Comparing in situ sensors for satellite validation, in *Geoscience and Remote Sensing Symposium (IGARSS), 2010 IEEE International*, pp. 699–701, IEEE, Honolulu, Hawaii, doi: 10.1109/IGARSS.2010.5652389.

Crow, W., and D. Ryu (2009), A new data assimilation approach for improving runoff prediction using remotely-sensed soil moisture retrievals, *Hydrol. Earth Syst. Sci.*, *13*(1), 1–16, doi:10.5194/hess-13-1-2009.

Crow, W. T., W. P. Kustas, and J. H. Prueger (2008), Monitoring root-zone soil moisture through the assimilation of a thermal remote sensing-based soil moisture proxy into a water balance model, *Remote Sens. Environ.*, *112*(4), 1268–1281, doi:10.1016/j.rse.2006.11.033.

Crow, W. T., A. A. Berg, M. H. Cosh, A. Loew, B. P. Mohanty, R. Panciera, P. de Rosnay, D. Ryu, and J. P. Walker (2012), Upscaling sparse ground-based soil moisture observations for the validation of coarse-resolution satellite soil moisture products, *Rev. Geophys.*, *50*, RG2002, doi:10.1029/2011RG000372.

De Lannoy, G. J., R. H. Reichle, P. R. Houser, V. Pauwels, and N. E. Verhoest (2007), Correcting for forecast bias in soil moisture assimilation with the ensemble Kalman filter, *Water Resour. Res.*, *43*, W09410, doi:10.1029/2006WR005449.

DeChant, C. M., and H. Moradkhani (2012), Examining the effectiveness and robustness of sequential data assimilation methods for quantification of uncertainty in hydrologic forecasting, *Water Resour. Res.*, *48*, W04518, doi:10.1029/2011WR011011.

Dee, D. P., and A. M. Da Silva (1998), Data assimilation in the presence of forecast bias, *Q. J. R. Meteorol. Soc.*, *124*(545), 269–295, doi: 10.1002/qj.49712454512.

Dong, J., S. C. Steele-Dunne, T. E. Ochsner, and N. van de Giesen (2015a), Determining soil moisture by assimilating soil temperature measurements using the ensemble Kalman filter, *Adv. Water Resour.*, *86*, 340–353, doi:10.1016/j.advwatres.2015.08.011.

Dong, J., S. C. Steele-Dunne, J. Judge, and N. van de Giesen (2015b), A particle batch smoother for soil moisture estimation using soil temperature observations, *Adv. Water Resour.*, *83*, 111–122, doi:10.1016/j.advwatres.2015.05.017.

Dong, J., S. C. Steele-Dunne, T. E. Ochsner, and N. van de Giesen (2016), Estimating soil moisture and soil thermal and hydraulic properties by assimilating soil temperatures using a particle batch smoother, *Adv. Water Resour.*, *91*, 104–116, doi:10.1016/j.advwatres.2016.03.008.

Draper, C., R. Reichle, G. De Lannoy, and Q. Liu (2012), Assimilation of passive and active microwave soil moisture retrievals, *Geophys. Res. Lett.*, *39*, L04401, doi:10.1029/2011GL050655.

Dumedah, G., and P. Coulibaly (2013), Evaluating forecasting performance for data assimilation methods: The ensemble Kalman filter, the particle filter, and the evolutionary-based assimilation, *Adv. Water Resour.*, *60*, 47–63, doi:10.1016/j.advwatres.2013.07.007.

Dunne, S., and D. Entekhabi (2005), An ensemble-based reanalysis approach to land data assimilation, *Water Resour. Res.*, *41*, W02013, doi: 10.1029/2004WR003449.

Entekhabi, D., I. Rodriguez-Iturbe, and F. Castelli (1996), Mutual interaction of soil moisture state and atmospheric processes, *J. Hydrol.*, *184*(1), 3–17, doi:10.1016/0022-1694(95)02965-6.
Entekhabi, D., E. G. Njoku, P. E. O'Neill, K. H. Kellogg, W. T. Crow, W. N. Edelstein, J. K. Entin, S. D. Goodman, T. J. Jackson, and J. Johnson (2010), The soil moisture Active Passive (SMAP) mission, *Proc. IEEE*, *98*(5), 704–716, doi:10.1109/JPROC.2010.2043918.
Evensen, G. (1994), Sequential data assimilation with a nonlinear quasi-geostrophic model using Monte Carlo methods to forecast error statistics, *J. Geophys. Res.*, *99*(C5), 10,143–10,162, doi:10.1029/94JC00572.
Evensen, G. (2009), *Data Assimilation: The Ensemble Kalman Filter*, pp. 119–137, Springer, N. Y.
Forman, B. A., and R. Reichle (2013), The spatial scale of model errors and assimilated retrievals in a terrestrial water storage assimilation system, *Water Resour. Res.*, *49*, 7457–7468, doi:10.1002/2012WR012885.
Forman, B. A., R. Reichle, and M. Rodell (2012), Assimilation of terrestrial water storage from GRACE in a snow-dominated basin, *Water Resour. Res.*, *48*, W01507, doi:10.1029/2011WR011239.
Kerr, Y. H., P. Waldteufel, J.-P. Wigneron, J. Martinuzzi, J. Font, and M. Berger (2001), Soil moisture retrieval from space: The Soil Moisture and Ocean Salinity (SMOS) mission, *IEEE Trans. Geosci. Remote Sens.*, *39*(8), 1729–1735, doi:10.1109/36.942551.
Larson, K. M., E. E. Small, E. D. Gutmann, A. L. Bilich, J. J. Braun, and V. U. Zavorotny (2008), Use of GPS receivers as a soil moisture network for water cycle studies, *Geophys. Res. Lett.*, *35*, L24405, doi:10.1029/2008GL036013.
Leisenring, M., and H. Moradkhani (2012), Analyzing the uncertainty of suspended sediment load prediction using sequential data assimilation, *J. Hydrol.*, *468*, 268–282, doi:10.1016/j.jhydrol.2012.08.049.
Liu, Y., and H. V. Gupta (2007), Uncertainty in hydrologic modeling: Toward an integrated data assimilation framework, *Water Resour. Res.*, *43*, W07401, doi:10.1029/2006WR005756.
Lu, S., T. Ren, Y. Gong, and R. Horton (2007), An improved model for predicting soil thermal conductivity from water content at room temperature, *Soil Sci. Soc. Am. J.*, *71*(1), 8–14, doi:10.2136/sssaj2006.0041.
Margulis, S., M. Girotto, G. Cortes, and M. Durand (2015), A particle batch smoother approach to snow water equivalent estimation a particle batch smoother approach to snow water equivalent estimation, *J. Hydrometeorol.*, 1752–1772, doi:10.1175/JHM-D-14-0177.1.
Margulis, S. A., D. McLaughlin, D. Entekhabi, and S. Dunne (2002), Land data assimilation and estimation of soil moisture using measurements from the southern great plains 1997 field experiment, *Water Resour. Res.*, *38*(12), 1299, doi:10.1029/2001WR001114.
McPherson, R. A., et al. (2007), Statewide monitoring of the mesoscale environment: A technical update on the Oklahoma mesonet, *J. Atmos. Oceanic Technol.*, *24*(3), doi:10.1175/JTECH1976.1.
Monsivais-Huertero, A., J. Judge, S. Steele-Dunne, and P.-W. Liu (2016), Impact of bias correction methods on estimation of soil moisture when assimilating active and passive microwave observations, *IEEE Trans. Geosci. Remote Sens.*, *54*(1), 262–278, doi:10.1109/TGRS.2015.2455037.
Montzka, C., H. Moradkhani, L. Weihermüller, H.-J. H. Franssen, M. Canty, and H. Vereecken (2011), Hydraulic parameter estimation by remotely-sensed top soil moisture observations with the particle filter, *J. Hydrol.*, *399*(3–4), 410–421, doi:10.1016/j.jhydrol.2011.01.020.
Montzka, C., J. P. Grant, H. Moradkhani, H.-J. H. Franssen, L. Weihermüller, M. Drusch, and H. Vereecken (2013a), Estimation of radiative transfer parameters from L-band passive microwave brightness temperatures using advanced data assimilation, *Vadose Zone J.*, *12*(3), doi:10.2136/vzj2012.0040.
Montzka, C., J. Grant, H.-J. Hendricks Franssen, M. Drusch, and H. Vereecken (2013b), A particle smoother with sequential importance resampling for radiative transfer parameter estimation, in *Geoscience and Remote Sensing Symposium (IGARSS), 2013 IEEE International*, pp. 3431–3434, IEEE, Vancouver, B. C., doi:10.1109/IGARSS.2013.6723566.
Moradkhani, H., S. Sorooshian, H. V. Gupta, and P. R. Houser (2005a), Dual state–parameter estimation of hydrological models using ensemble Kalman filter, *Adv. Water Resour.*, *28*(2), 135–147, doi:10.1016/j.advwatres.2004.09.002.
Moradkhani, H., K.-L. Hsu, H. Gupta, and S. Sorooshian (2005b), Uncertainty assessment of hydrologic model states and parameters: Sequential data assimilation using the particle filter, *Water Resour. Res.*, *41*, W05012, doi:10.1029/2004WR003604.
Moradkhani, H., C. M. DeChant, and S. Sorooshian (2012), Evolution of ensemble data assimilation for uncertainty quantification using the particle filter-Markov chain Monte Carlo method, *Water Resour. Res.*, *48*, W12520, doi:10.1029/2012WR012144.
Noh, S. J., O. Rakovec, A. H. Weerts, and Y. Tachikawa (2014), On noise specification in data assimilation schemes for improved flood forecasting using distributed hydrological models, *J. Hydrol.*, *519*, 2707–2721, doi:10.1016/j.jhydrol.2014.07.049.
Ochsner, T. E., M. H. Cosh, R. H. Cuenca, W. A. Dorigo, C. S. Draper, Y. Hagimoto, Y. H. Kerr, E. G. Njoku, E. E. Small, and M. Zreda (2013), State of the art in large-scale soil moisture monitoring, *Soil Sci. Soc. Am. J.*, *77*(6), 1888–1919, doi:10.2136/sssaj2013.03.0093.
Oleson, K. W., D. M. Lawrence, G. B. Bonan, M. G. Flanner, E. Kluzek, P. J. Lawrence, S. Levis, S. C. Swenson, and P. E. Thornton (2010), Technical description of version 4.0 of the community land model (CLM), NCAR Tech. Note NCAR/TN-478+STR, pp. 61–72.
Owe, M., R. de Jeu, and T. Holmes (2008), Multisensor historical climatology of satellite-derived global land surface moisture, *J. Geophys. Res.*, *113*, F01002, doi:10.1029/2007JF000769.
Qin, J., S. Liang, K. Yang, I. Kaihotsu, R. Liu, and T. Koike (2009), Simultaneous estimation of both soil moisture and model parameters using particle filtering method through the assimilation of microwave signal, *J. Geophys. Res.*, *114*, D15103, doi:10.1029/2008JD011358.
Rafieeinasab, A., D.-J. Seo, H. Lee, and S. Kim (2014), Comparative evaluation of maximum likelihood ensemble filter and ensemble Kalman filter for real-time assimilation of streamflow data into operational hydrologic models, *J. Hydrol.*, *519*, 2663–2675, doi:10.1016/j.jhydrol.2014.06.052.
Rakovec, O., A. Weerts, P. Hazenberg, P. Torfs, and R. Uijlenhoet (2012), State updating of a distributed hydrological model with ensemble Kalman filtering: Effects of updating frequency and observation network density on forecast accuracy, *Hydrol. Earth Syst. Sci.*, *16*(9), 3435–3449, doi:10.5194/hess-16-3435-2012.
Rawls, W., D. Brakensiek, and K. Saxton (1982), Estimation of soil water properties, *Trans. ASAE*, *25*(5), 1316–1320, doi:10.13031/2013.33720.
Reichle, R. H. (2008), Data assimilation methods in the Earth sciences, *Adv. Water Resour.*, *31*(11), 1411–1418, doi:10.1016/j.advwatres.2008.01.001.
Reichle, R. H., and R. D. Koster (2005), Global assimilation of satellite surface soil moisture retrievals into the NASA catchment land surface model, *Geophys. Res. Lett.*, *32*, L02404, doi:10.1029/2004GL021700.
Reichle, R. H., R. D. Koster, J. Dong, and A. A. Berg (2004), Global soil moisture from satellite observations, land surface models, and ground data: Implications for data assimilation, *J. Hydrometeorol.*, *5*(3), 430–442, doi:10.1175/1525-7541(2004)005<0430:GSMFSO>2.0.CO;2.
Ryu, D., W. T. Crow, X. Zhan, and T. J. Jackson (2009), Correcting unintended perturbation biases in hydrologic data assimilation, *J. Hydrometeorol.*, *10*(3), 734–750, doi:10.1175/2008JHM1038.1.
Saito, H., J. Šimnek, and B. P. Mohanty (2006), Numerical analysis of coupled water, vapor, and heat transport in the Vadose zone, *Vadose Zone J.*, *5*(2), 784, doi:10.2136/vzj2006.0007.
Sayde, C., C. Gregory, M. Gil-Rodriguez, N. Tufillaro, S. Tyler, N. van de Giesen, M. English, R. Cuenca, and J. S. Selker (2010), Feasibility of soil moisture monitoring with heated fiber optics, *Water Resour. Res.*, *46*, W06201, doi:10.1029/2009WR007846.

Schaap, M. G., F. J. Leij, and M. T. van Genuchten (2001), Rosetta: A computer program for estimating soil hydraulic parameters with hierarchical pedotransfer functions, *J. Hydrol.*, *251*(3), 163–176, doi:10.1016/S0022-1694(01)00466-8.

Selker, J. S., L. Thévenaz, H. Huwald, A. Mallet, W. Luxemburg, N. van De Giesen, M. Stejskal, J. Zeman, M. Westhoff, and M. B. Parlange (2006), Distributed fiber-optic temperature sensing for hydrologic systems, *Water Resour. Res.*, *42*, W12202, doi:10.1029/2006WR005326.

Sellers, P. J. (1985), Canopy reflectance, photosynthesis and transpiration, *Int. J. Remote Sens.*, *6*(8), 1335–1372, doi:10.1080/01431168508948283.

Simunek, J., M. Sejna, H. Saito, M. Sakai, and M. T. Van Genuchten (2009), *The HYDRUS-1D Software Package for Simulating the One-Dimensional Movement of Water, Heat, and Multiple Solutes in Variably-Saturated Media*, Univ. of Calif., Riverside, pp. 11–52.

Steele-Dunne, S. C., M. M. Rutten, D. M. Krzeminska, M. Hausner, S. W. Tyler, J. Selker, T. a. Bogaard, and N. C. van de Giesen (2010), Feasibility of soil moisture estimation using passive distributed temperature sensing, *Water Resour. Res.*, *46*, W03534, doi:10.1029/2009WR008272.

Striegl, A. M., S. P. Loheide, and S. P. Loheide II (2012), Heated distributed temperature sensing for field scale soil moisture monitoring, *Ground Water*, *50*(3), 340–7, doi:10.1111/j.1745-6584.2012.00928.x.

Su, H., Z.-L. Yang, G.-Y. Niu, and C. R. Wilson (2011), Parameter estimation in ensemble based snow data assimilation: A synthetic study, *Adv. Water Resour.*, *34*(3), 407–416, doi:10.1016/j.advwatres.2010.12.002.

Van Genuchten, M. T. (1980), A closed-form equation for predicting the hydraulic conductivity of unsaturated soils, *Soil Sci. Soc. Am. J.*, *44*(5), 892–898, doi:10.2136/sssaj1980.03615995004400050002x.

Van Leeuwen, P. J., and G. Evensen (1996), Data assimilation and inverse methods in terms of a probabilistic formulation, *Mon. Weather Rev.*, *124*(12), 2898–2913, doi:10.1175/1520-0493(1996)124<2898:DAAIMI>2.0.CO;2.

Vrugt, J. A., C. J. ter Braak, C. G. Diks, and G. Schoups (2013), Hydrologic data assimilation using particle Markov chain Monte Carlo simulation: Theory, concepts and applications, *Adv. Water Resour.*, *51*, 457–478, doi:10.1016/j.advwatres.2012.04.002.

Wagner, W., G. Lemoine, M. Borgeaud, and H. Rott (1999), A study of vegetation cover effects on ERS scatterometer data, *IEEE Trans. Geosci. Remote Sens.*, *37*(2), 938–948, doi:10.1109/36.752212.

Yan, H., C. M. DeChant, and H. Moradkhani (2015), Improving soil moisture profile prediction with the particle filter-Markov Chain Monte Carlo method, *IEEE Trans. Geosci. Remote Sens.*, *50*, 6134–6147, doi:10.1109/TGRS.2015.2432067.

Yu, Z., D. Liu, H. Lü, X. Fu, L. Xiang, and Y. Zhu (2012), A multi-layer soil moisture data assimilation using support vector machines and ensemble particle filter, *J. Hydrol.*, *475*, 53–64, doi:10.1016/j.jhydrol.2012.08.034.

Zaitchik, B. F., M. Rodell, and R. H. Reichle (2008), Assimilation of grace terrestrial water storage data into a land surface model: Results for the Mississippi River Basin, *J. Hydrometeorol.*, *9*(3), 535–548, doi:10.1175/2007JHM951.1.

Zreda, M., D. Desilets, T. Ferré, and R. L. Scott (2008), Measuring soil moisture content non-invasively at intermediate spatial scale using cosmic-ray neutrons, *Geophys. Res. Lett.*, *35*, L21402, doi:10.1029/2008GL035655.